pyESDv1.0.1: An open-source Python framework for empirical-statistical downscaling of climate information

Daniel Boateng*, Sebastian G. Mutz

5   Department of Geosciences, University of Tübingen, Tübingen, Germany

* Correspondence to: daniel.boateng@uni-tuebingen.de

Abstract. The nature and severity of climate change impacts vary significantly from region to region. Consequently, high-
10   resolution climate information is needed for meaningful impact assessments and the design of mitigation strategies. This
demand has led to an increase in the coupling of Empirical Statistical Downscaling (ESD) models to General Circulation
Model (GCM) simulations of future climate. In contrast to dynamical downscaling, the Perfect Prognosis ESD (PP-ESD)
approach has several benefits, including low computation costs, the prevention of the propagation of GCM specific errors, and
high compatibility with different GCMs. Despite their advantages, the use of ESD models and the resulting data products is
15   hampered by (1) the lack of accessible and user-friendly downscaling software packages that implement the entire downscaling
cycle, (2) difficulties to reproduce existing data products and assess their credibility, and (3) difficulties to reconcile different
ESD-based predictions for the same region. We address these issues with a new open-source Python PP-ESD modeling
framework *pyESD*. pyESD implements the entire downscaling cycle, i.e., routines for data preparation, predictor selection and
construction, model selection and training, evaluation, utility tools for relevant statistical tests, visualization, and more. The
20   package includes a collection of well-established Machine Learning algorithms and allows the user to choose a variety of
estimators, cross-validation schemes, objective function measures, hyperparameter optimization, etc., in relatively few lines
of code. The package is well documented, highly modular, and flexible. It allows quick and reproducible downscaling of any
climate information, such as precipitation, temperature, wind speed, or even short-term glacier length and mass changes. We
demonstrate the use and the effectiveness of the new PP-ESD framework by generating weather station-based downscaling
25   products for precipitation and temperature in complex mountainous terrain in Southwest Germany. The application example
covers all important steps of the downing cycle and different levels of experimental complexity. All scripts and datasets used
in the case study are publicly available to (1) ensure the reproducibility and replicability of the modeled results, and (2) simplify
learning to use the software package.

1 Introduction

The impacts of anthropogenic climate change are far-reaching and spatially heterogeneous. Consequently, regional and local
scale predictions of 21st century climate evolution are needed to help guide the design of adaptation measures, vulnerability
assessments, and resilience strategies (Field and Barros, 2014; Weaver et al., 2013). General Circulation Models (GCMs) are
well-established tools for simulating climate trends in response to different anthropogenic and natural forcings, such as
atmospheric CO_2 concentrations, land cover, and orbital changes. They are process-driven models, based on our understanding
of atmospheric physics. They are commonly used to predict future trends of climate change by prescribing predicted future
forcings described by the Representative Concentration Pathways (RCPs). RCPs are greenhouse gas concentration scenarios
that quantify the radiative forcing of plausible demographic and technological developments, and anthropogenic activities
(Meinshausen et al., 2011; Pachauri et al., 2014). While GCMs can produce accurate estimates of many climate system
elements on the global and synoptic scale (such as circulation patterns), mesoscale atmospheric processes, clouds, and specific
climate variables like precipitation are still relatively poorly represented (e.g., Steppeler et al., 2003). Moreover, GCM
simulations are affected by systematic biases on the local and regional scale due to their coarse resolutions and model
parameterization (e.g., Errico et al., 2001). These can lead to inaccurate predictions on the spatial scales that are relevant for
regional climate change impact assessments, such as studies investigating the impacts on the hydrological cycle (Boé et al.,
2009), mountain glaciers (Mutz et al., 2015; Mutz and Aschauer, 2022), air quality (e.g., Colette et al., 2012) and agriculture
(e.g., Shahhosseini et al., 2020). Therefore, GCM-based predictions are downscaled by performing dynamical downscaling or
Empirical Statistical Downscaling (ESD) (Murphy, 2000; Schmidli et al., 2007; Wilby and Dawson, 2013).

Dynamical downscaling involves the nesting of Regional Climate Models (RCMs) into coarse-resolution GCM simulations to
produce higher resolution regional estimates. While RCMs allow an easy exploration of physical processes leading to the
predicted climate, they are computationally costly. Furthermore, slight changes in the model domain and boundary conditions
require the repetition of the whole process, thereby limiting their application in many climate impact studies (e.g., Giorgi and
Mearns, 1991; Xu et al., 2019). ESD is computationally less costly and implicitly considers local conditions, such as
topography and vegetation, without the need to parameterize them explicitly. It is widely used for climate change impact
studies and relies on establishing empirical transfer functions to relate large-scale atmospheric variables (predictors) to a local-
scale observation (predictand). ESD models can be directly coupled to GCMs (e.g. Mutz et al., 2021) or RCMs (e.g., Sunyer
et al., 2015; Laflamme et al., 2016; Jakob Themeßl et al., 2011). ESD can be broadly categorized into Perfect Prognosis (PP)
and Model Output Statistics (MOS) approaches (Maraun and Widmann, 2018; Marzban et al., 2006). MOS uses simulated
predictors from the GCM or RCM to find the transfer function and generate a predictand time series with bias corrections (e.g.,
Sachindra et al., 2014; Wilby et al., 1998). Therefore, the MOS-ESD transfer functions are specific to a particular GCM or
RCM and not easily transferable to other models. In contrast, the PP-ESD approach is GCM- and RCM-agnostic: ESD models
are obtained from observational data for both the predictand and predictors, and can therefore be coupled to any GCM or RCM

65 (e.g., Hertig et al., 2019; Mutz et al., 2021; Ramon et al., 2021; Tatli et al., 2004). Therefore, this paper, and the software package presented in it, focuses primarily on the PP-ESD approach.

The PP-ESD modeling framework consists of four critical steps to establish and evaluate the empirical transfer functions that constitute an ESD model (e.g., Maraun et al., 2010; Maraun and Widmann, 2018): (1) The first step involved the selection and construction of predictors. The selection of the most informative and relevant predictors generally increases the performance

70 and robustness of the PP-ESD models. Preliminary predictor selection should be guided by knowledge of the atmospheric dynamics that govern a specific regional climate. This selection may be refined using statistical dependency measures such as correlation analysis (e.g., Wilby et al., 2002; Wilby and Wigley, 2002), regularization regression (e.g., Hammami et al., 2012), stepwise multi-linear regression (e.g., Mutz et al., 2021) and decision tree selection (e.g., Nourani et al., 2019). The selected predictors should be able to explain most of the predictand's variability and must be represented well by the GCMs (Maraun

75 and Widmann, 2018; Wilby et al., 2004). (2) The second step involves the selection of the learning algorithms (i.e., the learning model used for training the ESD model). These range from classical regressions and analog models, including parametric and non-parametric models (Gutiérrez et al., 2013; Zorita and Storch, 1999; Lorenz, 1969), to advanced Machine Learning (ML) algorithms (e.g., Sachindra et al., 2018; Xu et al., 2020). The various techniques vary in complexity, scalability, interpretability, and underlying assumptions. For example, classical regressions and analog models allow better interpretations of the simulated

80 results, and are usually simpler to implement. On the other hand, several ML algorithms have the ability to capture more complex links between predictors and predictand, and do not require an explicit assumption of the distribution of observational data during the optimization process (Jordan and Mitchell, 2015; Raissi and Karniadakis, 2018). The choice of the optimal PP-ESD training technique depends on the predictand variable (e.g., precipitation and temperature), length of the observational records, spatiotemporal variability, spatial coherence, regional setting, and the temporal stationarity of the transfer functions.

85 (3) The third step involves the actual training and validation of the PP-ESD models, and (4) the final step is the PP-ESD model evaluation.

The high demand for climate change information on the regional and local scale has led to the widespread use of ESD methods and an overwhelming body of research to sort through in order to select the most suitable technique for a specific problem. In the past, Generalized Linear Models (GLMs) (e.g., Fealy and Sweeney, 2007), regularization models (e.g., Li et al., 2020),

90 Bayesian regression models (Das et al., 2014; e.g., Zhang and Yan, 2015), Support Vector Machines (SVM) (e.g., Chen et al., 2010; Ghosh and Mujumdar, 2008), Artificial Neural Networks (ANNs) (e.g., Sachindra et al., 2018; Vu et al., 2016; Xu et al., 2020), homogeneous (e.g., Random Forest) and heterogeneous (e.g., Stacking) ensemble learning models (e.g., Massaoudi et al., 2021; Pang et al., 2017; Zhang et al., 2021), and others have been used to construct PP-ESD models and downscale climate information. However, there is no universal protocol to help choose a robust model for a specific region and climate

95 variable (Gutiérrez et al., 2019), thus making the selection of the most suited learning algorithm challenging. Moreover, the recent increase in ML algorithms and platforms (e.g., programming languages and software) exacerbates the problem by creating an even wider range of PP-ESD techniques without well-defined protocols. These have shifted the focus toward the establishment of standardized user-friendly tools that would resolve most of the issues related to the development of PP-ESD

models. Such tools exist in various forms and tackle a certain aspect of the inherent ESD modeling complexities to ensure fast
100   and efficient climate impact-related studies. For example, the R-package *esd*, developed and maintained by the Norwegian
Meteorological Institute (MET Norway), comprises many utility functions for data retrieval, manipulation and visualization,
commonly used statistical tools, and implementations of GLM and regression techniques for generating ESD models (Benestad
et al., 2015). Moreover, an interactive web-based downscaling tool developed as part of the EU-funded ENSEMBLES project
(van der Linden and Mitchell, 2009) provides an end-to-end framework through data access, computing resources and ESD
105   model alternatives (Gutiérrez et al., 2012). The decision support tool *sdsm* (Wilby et al., 2002) provides auxiliary downscaling
routines like predictor screening, regression, model evaluation, and visualization for near-surface weather variables on a daily
scale. Most recently, the climate analysis tool *Climate4R* has been extended with statistical downscaling functionalities
(*downscaleR*) that provide a wide range of MOS and PP techniques (Bedia et al., 2020). While these tools provide specialist
solutions, there is no single tool or modeling framework that provides a wide range of contemporary (and commonly used)
110   algorithms and implements all downscaling steps (i.e., predictors selection and construction, learning algorithm selection,
training and validation of ESD models, GCM-ESD model coupling, model evaluation, visualization, and relevant statistical
tools). Moreover, there is no user-friendly ESD tool written in a widely used programming language like Python, which would
remove barriers for the use of ESD techniques in research and teaching. A complete, user-friendly, robust and efficient open-
source downscaling framework would contribute significantly to climate change impact assessment studies by (a) empowering
115   researchers through accessible software and easy switches between alternative methods, (b) allowing for efficient updating of
predictions in a consistent modeling framework, (c) increasing the transparency and reproducibility of results, and by (d)
removing barriers in teaching in order to familiarize future generations of researchers with the ESD approach.

Here, we introduce a new PP-ESD framework that addresses the gaps highlighted above. It is a thoroughly tested, heavily
documented, efficient, and user-friendly open-source Python Empirical Statistical Downscaling (*pyESD*) package. *pyESD*
120   adopts an Object Oriented Programming (OOP) style and treats the predictand data archives (e.g., the weather station) as
objects with many functionalities and attributes relevant to ESD modeling. It is flexible with regards to the training dataset
and predictand variable. For example, *pyESD*'s predecessors were successfully applied for the prediction of local temperatures
(Mutz et al., 2021) and glacier mass balance (Mutz and Aschauer, 2022) in South America. Here, we additionally demonstrate
its capabilities in downscaling precipitation in complex terrain in Southwest Germany. *pyESD* comprises a collection of
125   utilities and methods for data preparation, predictor selection, data transformation, predictor construction, model selection and
training, evaluation, statistical testing, and visualization. Unlike the existing packages, *pyESD* also includes common machine
learning algorithms (i.e., different estimators, cross-validation schemes, objective function measures, hyperparameter
optimizers, etc.) that can be experimented with in a few lines of code.

In the first part of this paper (Section 2), we provide detailed descriptions of the model structure and the theoretical background
130   for the implemented methods. In the second part (Section 3), we demonstrate the package's functionalities with an illustrative
case study for a hydrological sub-catchment in mountainous terrain in Southwest Germany. Here, we walk the reader through
a typical downscaling process with *pyESD*. More specifically, we generate station-based downscaling products for

precipitation and temperature changes in response to different RCPs. When discussing downscaling-related tasks, we list the corresponding *pyESD* routines as italicized function names. We only use publicly available data for a set of weather stations

135 to ensure the reproducibility and replicability of the results (see Section 3). Moreover, all the scripts used for the case study are provided and can be easily adapted to suit the researcher's focus. We discuss the application example in Section 4 and conclude with a summary and important remarks in Section 5.

2 Model structure

The PP-ESD downscaling cycle involves technical and laborious steps that must be carefully addressed to ensure the robustness

140 and accuracy of local-scale climate predictions. The *pyESD* package implements all these steps in an efficient modeling pipeline for an easier workflow. In this section, we describe this workflow (Fig. 1) along with the main features of the package.
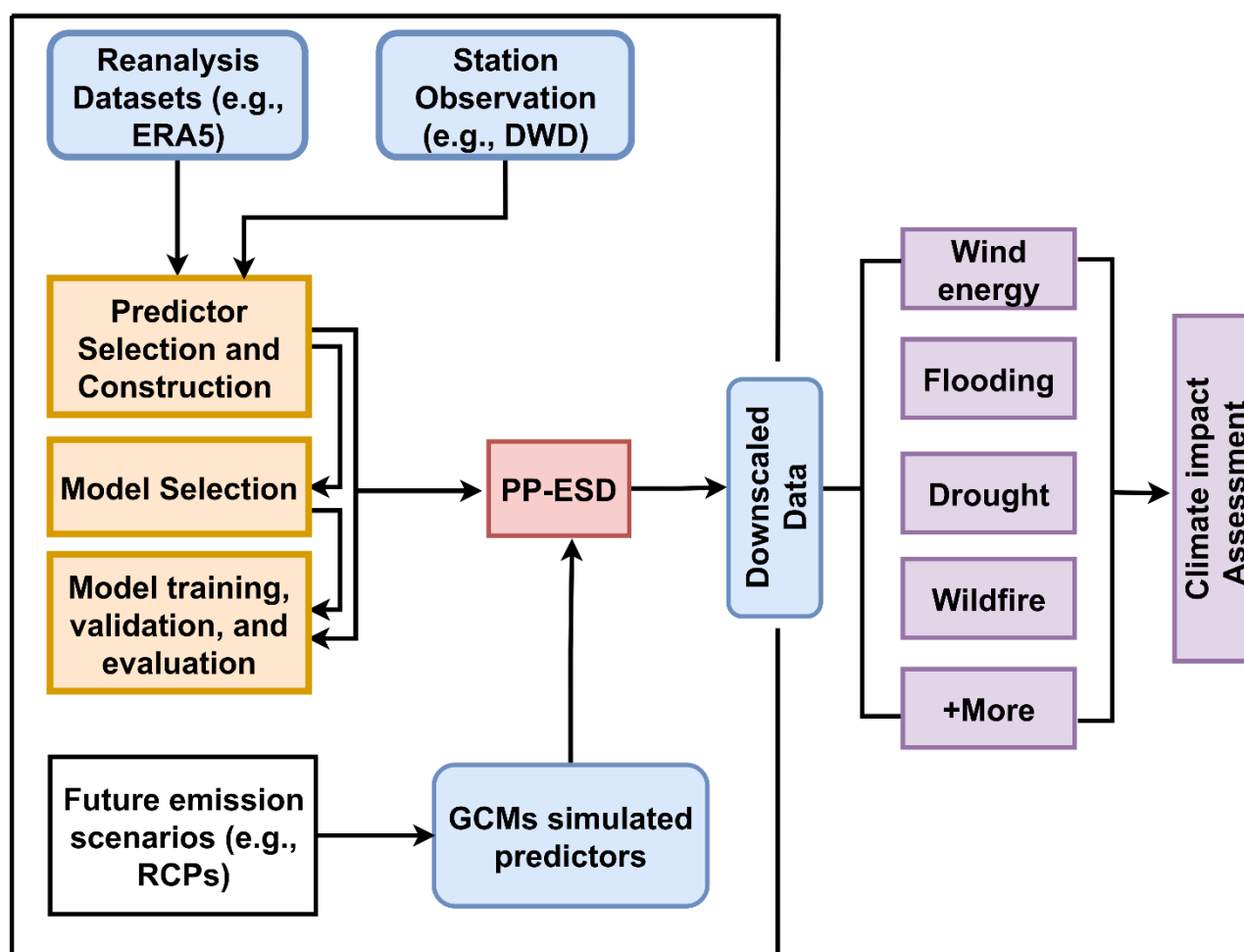
Fig. 1: The main features and workflow of PP-ESD implemented in the pyESD package. The weather station and reanalysis datasets are used to select the robust predictors for model training and validation. The trained PP-ESD model is then coupled to GCMs
145 **simulations forced with different scenarios to predict the local-scale future estimates that can be used for climate change impact assessment (not included in the pyESD package).**

2.1 Data structure and preprocessing

PP-ESD modeling requires (1) predictand data from weather stations or other observational systems, (2) reanalysis datasets for the construction of predictors, and (3) GCM or RCM output for the construction of simulated predictors if the PP-ESD
150 models are used for downscaling simulated climates. To understand the workflow demonstrated in later sections, the reader needs to be aware of few important package design choices related to data structure and preprocessing:

- The package adopts the OOP paradigm and treats every predictand data archive (e.g., weather station or glacier) as an object. Since the current version of the package focuses only on station-based downscaling, we will henceforth describe it only as the weather station object. The package accepts the (for weather stations typical) Comma Separated
155 Values (CSV) file format. These files contain the predictand time series, such as a temperature record, as well as weather station attributes like the weather station's name, ID, and location. The *read_station_csv* from *pyESD.weatherstation* module initiates each weather station as a separate object using the S*tationOperator* that features all the other functionalities. The weather station object is associated with at least one predictand dataset (i.e., the values of at least one climate variable recorded at that particular station). Furthermore, the initialized object
160 includes all attributes and methods required for the complete downscaling cycle. For instance, the package adopts the *fit* and *predict* framework of the scikit-learn python package (Pedregosa et al., 2011) that can be directly applied to the weather station object.

- The data needed for predictor construction is read from files in the network Common Data Form (netCDF) format with the *xarray* toolkit (Hoyer and Hamman, 2017). Due to the size of these datasets and the computations required
165 to construct the predictors, the memory demand can be very high, and repeating this step every time a new model is trained or applied becomes computationally very costly. This problem is circumvented by storing the constructed predictors for each weather station stored in *pickle* files. At next runtime, these can quickly be read (or unpacked) to reduce the computational costs and facilitate faster experimentation with the package.

- Since reanalysis datasets, climate model output, and weather station data are provided by different data centers and
170 have varied structures and attributes, it is well outside the scope of our project to write and include a unified data processing function for all. Instead, the pre-processing functions of the current version of *pyESD* are written for state-of-the-art, representative and publicly available datasets. More specifically, they work with weather station data from the German Weather Service (Deutscher Wetterdienst, DWD) and the ERA5 reanalysis product (Hersbach et al., 2020). These preprocessing functions are provided as part of the package utilities (*pyESD.data_preprocess_utils*) and
175 can easily be adapted to work for the researchers' preferred datasets. The functions will be expanded in the future to

allow experimentation with other popular datasets and assess the sensitivity of ESD model performance to the choice of reanalysis datasets (e.g., Brands et al., 2012).

2.2 Predictor selection and construction

The PP-ESD approach is highly sensitive to the choice of predictors and learning models (Maraun et al., 2019; Gutiérrez et al., 2019). Moreover, since PP-ESD models are empirical in nature, the predictors serve as proxies for all the relevant physical processes and must be informative enough to account for the local predictand variability (Huth, 1999, 2004; Maraun and Widmann, 2018). Therefore, the selection of potential predictors should be informed by our knowledge of the atmospheric dynamics that control the climate variability of the study area. For example, synoptic-scale climate features, such as atmospheric teleconnection patterns, control much of the regional-scale climate variability. It is therefore recommended to consider these as potential predictors. Statistical techniques, such as methods for feature selection or dimension reduction, may then be applied to reduce the list of physically relevant potential predictors to a smaller selection of predictors that have a robust statistical relationship with the predictand. These steps contribute to the performance of the models and also resolve some of the issues related to multicollinearity and overfitting (e.g., Mutz et al., 2015). The *pyESD* package adopts three different wrapper feature selection techniques that can be explored for different models: (1) Recursive feature elimination (Chen and Jeong, 2007), (2) Tree-based feature selection (Zhou et al., 2021), and (3) Sequential feature selection (Ferri et al., 1994). The methods are included in *pyESD.feature_selection* as *RecursiveFeatureElimination*, *TreeBasedSelection,* and *SequetialFeatureSelection*, respectively. Furthermore, classical filter feature selection techniques, such as correlation analyses, are also included as a method of the weather station object.

Predictors are typically constructed by (1) computing the regional means of a physically relevant climate variable, or (2) by constructing index time series for relevant synoptic-scale climate phenomena. The package allows the user to consider a few important aspects for each type of predictor:

1. The area over which the climate variable is averaged can significantly affect model performance. In complex terrain with high-frequency topography, for example, choosing a smaller spatial extent may result in the predictor having a higher explanatory power. Therefore, a radius (with a default value of 200 km) around the weather station may be defined by the user to determine the size of the area used for the computation of the regional means.

2. EOF analysis is a well-established tool for capturing atmospheric teleconnection patterns and reducing high-dimensional climate datasets to index time series that represent the variability of prominent modes of synoptic-scale climate phenomena (Storch and Zwiers, 2002). The current version of *pyESD* includes functions for the extraction of EOF-based index time series for dominant extra-tropical teleconnection patterns in the Northern Hemisphere (*pyESD.teleconnections*). More specifically, it allows the computation of index values for the North Atlantic Oscillation (NAO), East Atlantic (EA), Scandinavian (SCAN), and East Atlantic/Western Russian (EAWR) oscillation patterns (e.g., Boateng et al., 2022). It will be expanded to consider Southern Hemisphere patterns in future versions.

After the selection and construction of predictors, their raw values can be transformed before model training. For instance, the

210 *MonthlyStandardizer* implemented in the *pyESD.standardizer* can be used to remove the seasonal trends in each predictor by centering and scaling the data. Such transformation can reduce biases toward high-variance predictors, ensure generalization, and improve the representation of predictors constructed from GCM output (e.g., Bedia et al., 2020; Benestad et al., 2015). Principal component analysis (PCA) is another transformation tool included in the package (*pyESD.standardizer.PCAScaling*). It can be applied to (a) reduce the raw predictor values to information that is relevant to the predictand, and (b) prevent

215 multicollinearity-related problems during model training (e.g. Mutz et al., 2015).

2.3 Learning Models

The empirical relationship between local predictand and large-scale predictors is often complicated due to the complex dynamics in the climate system. However, ML algorithms have been demonstrated to perform well in extracting hidden patterns in climate data that are relevant for building more complex transfer functions (e.g., Raissi and Karniadakis, 2018).

220 Specifically, neural networks have been explored for downscaling climate information due to their ability to establish a complex and nonlinear relationship between predictand and predictors (e.g., Nourani et al., 2019; Gardner and Dorling, 1998; Vu et al., 2016). Moreover, Support Vector Machine (SVM) models have been used to capture the links between predictors and predictand by mapping the low-dimensional data into a high-dimensional feature space with the use of kernel functions (e.g. Anandhi et al., 2008; Tripathi et al., 2006). Previous studies have also applied multi-model ensembles due to their ability

225 to reduce model variance and capture the distribution of the training data (e.g., Xu et al., 2020; Massaoudi et al., 2021; Gu et al., 2022).

Selecting the most appropriate model or algorithm for a specific location or predictand can be challenging, because one needs to consider many case-specific factors like data dimensionality, distribution, temporal resolution, and explainability. This problem is exacerbated by the lack of well-established frameworks for climate information downscaling (Gutiérrez et al.,

230 2019). The *pyESD* package addresses this challenge with the implementation of many ML models that are different with regard to their theoretical paradigms, assumptions and model structure. The implementation of commonly used models in the same package allows researchers to experiment with different learning models, and to replicate and update their research based on emerging recommendations for specific predictands and geographical locations. The implementation of statistical and ML models in *pyESD* mainly relies on the open-source scientific framework scikit-learn tool (Pedregosa et al., 2011). In the

235 following subsections, we briefly explain the principles behind the ML methods that are included in the *pyESD* package.

2.3.1 Regularization regressors

Regularization models are penalized regression techniques that shrink the coefficients of uninformative predictors to improve model accuracy and prediction interpretability (Hastie et al., 2001; Tibshirani, 1996; Gareth et al., 2013). The coefficients of non-robust predictors are set to zero by minimizing the absolute values of regression coefficients or minimizing the sum of

240 squares of the coefficients. The former is referred to as L1 regularization and adopted by the Least Absolute Shrinkage and

Selection Operator (LASSO) method. The latter is referred to as L2 regularization and adopted by the Ridge regression method. The regularization term (R) and the updated cost function for a linear equation of p independent variables or predictors, X_i are defined as:

$$R(\beta) = \sum_{i=1}^{p} |\beta_i| \tag{1}$$

245   for L1 regularization, and

$$R(\beta) = \sum_{i=1}^{p} \beta_i^2 \tag{2}$$

for L2 regularization. Therefore, the updated cost function is defined:

$$cost = \sum_{j=1}^{n} \left(y_j - \sum_{i=1}^{p} X_{ij}\beta_i \right)^2 + \lambda R(\beta), \tag{3}$$

where λ is the tuning parameter that controls the severity of the penalty defined in Eqs. (1) and (2), and β_i are the coefficients.

250   The package features implementations of the LASSO and Ridge regression using a cross-validation (CV) scheme with random bootstrapping to iteratively optimize λ. These are included as *LassoCV* and *RidgeCV*, respectively. The optimization of the cost function in Eqs. (3) is usually based on the coordinate descent algorithm to fit the coefficients (Wu and Lange, 2008). The *pyESD* package also includes an implementation of *LassoCV* that uses a less greedy version of the optimizer (*LassoLarsCV*). It is computationally more efficient by using the least angle regression (Efron et al., 2004) for fitting the coefficients.

255   **2.3.2 Bayesian Regression**

Bayesian regression employs a type of conditional modeling to obtain the posterior probability (p) of the target variable (y), given a combination of predictor variables (X), regression coefficients (w) and random variable (α) estimated from the data (Bishop and Nasrabadi, 2006; Neal, 2012). In its simplest form, the normal linear model, the predictand y_i (given the predictors X_j), follows a Gaussian distribution $N(\mu, \sigma)$. Therefore, to estimate the full probabilistic model, y_i is assumed to be normally

260   distributed around $X_{ij}w$:

$$p(y_i \mid X, w, \alpha) = N\big(y_i \mid X_{ij}w, \alpha\big) \tag{4}$$

This approach also permits the use of regularizers in the optimization process. The Bayesian Ridge regression procedure (*BayesianRidge*) estimates the regression coefficients from a spherical Gaussian and L2 regularization (Eqs. (2)). The regularizer parameters (α, λ) are estimated by maximizing the log marginal likelihood under a Gaussian prior over w with a

265   precision of λ^{-1} (Tipping, 2001; MacKay, 1992):

$$p(w|\alpha) = N\big(w \mid 0, \lambda^{-1}I_p\big) \tag{5}$$

This means that the parameters (α, λ, w in Eqs. (4) and (5)) are estimated jointly in the calibration process. The Automatic Relevance Determination regression (*ARD*) is an alternative model included in the package. It differs from *BayesianRidge* in estimating sparse regression coefficients and using centered elliptic Gaussian priors over the coefficients w (Wipf and Nagarajan, 2007; Tipping, 2001). Previous studies have used sparse Bayesian learning (Relevance Vector Machine (RVM)) for downscaling climate information (e.g., Das et al., 2014; Ghosh and Mujumdar, 2008).

2.3.3 Artificial Neural Network

The MultiLayer Perceptron (MLP) is a classical example of a feedforward ANN (Gardner and Dorling, 1998; Pal and Mitra, 1992). MLP is a supervised learning algorithm that consists of three layers (i.e., an input, hidden, and output layer) connected by transformation coefficients (weights) using non-linear activation such as the hyperbolic function. More specifically, the learning algorithm with one hidden layer for the training sets $(X_1, y_1), (X_2, y_2), \ldots, (X_n, y_n)$ where $X_i \epsilon R^n$, and $y_i \epsilon \{0,1\}$, can be defined as:

$$f(X) = W_2 \theta \left(W_1^T X + b_1 \right) + b_2, \tag{6}$$

where θ is the activation function, and b_1, b_2 are the model biases added to the hidden and output layer. The weights connecting the layers are optimized with the backpropagation algorithm (Hecht-Nielsen, 1992; Rumelhart et al., 1986) with a mean squared error loss function. Moreover, the L2 regularization (Eqs. (2)) method is applied to avoid overfitting by shrinking the weights with higher magnitudes. Therefore, the optimized squared error loss function is defined as:

$$Loss(\hat{y}, y, W) = \frac{1}{2} \|\hat{y} - y\|_2^2 + \frac{\alpha}{2} \|W\|_2^2, \tag{7}$$

where the $\frac{\alpha}{2} \|W\|_2^2$ is the L2 penalty that shrinks the model complexity. Often, the derivative of the loss function with respect to the weights is determined until the residual error of the model is satisfactory. The stochastic gradient descent algorithm (Bottou, 1991; Kingma and Ba, 2014) is used as a solver for updating the weights (defined in Eqs. (6)) in a maximum number of iterations until a satisfactory loss (Eqs. (7)) is achieved. Moreover, the choice of the parameters, such as the size of hidden layers, activation function, and learning algorithm, is relevant to the performance of the model (Diaz et al., 2017). The exhaustive search algorithm with CV bootstrapping is a simple and efficient method for parameter optimization (Pontes et al., 2016) and therefore included in the *pyESD* package (*GridSearchCV*).

2.3.4 Support Vector Machine

The Support Vector Regression (SVR) uses the principles of SVM as a regression technique. The learning algorithms are based on Vapnik–Chervonenkis (VC) theory and empirical risk minimization that is designed to solve linear and non-linear problems. This is achieved by applying kernel functions to map low dimensional data to higher or even infinite dimensional feature space (Vapnik, 1999; Cristianini and Shawe-Taylor, 2000). In principle, the model creates a hyperplane in a vector space containing groups of data points. This hyperplane is a linear classifier that maximizes the group margins. Given finite predictor and predictand data points $(X_1, y_1), (X_2, y_2), \ldots, (X_n, y_n)$ where $X_i \epsilon R^n$, and $y_i \epsilon R$, the regressor can be defined as:

$$f(X, w) = w^T \phi(X) + b, \tag{8}$$

where the support vectors w and model bias b are the optimal parameters that minimize the cost function in Eqs. (9).

$$cost = \frac{1}{2} w^T w + C \sum_{i=1}^{n} (\xi_i + \hat{\xi}_i), \tag{9}$$

$$subject\ to\ \{y_i - f(X_i, w) \leq \varepsilon + \hat{\xi}_i, f(X_i, w) - y_i \leq \varepsilon + \xi_i\},$$

where $\xi_i, \hat{\xi}_i \geq 0, i = 1 \dots n$, are the slack variables (the upper and lower training errors) subject to the error tolerance of ε that prevents overfitting. C represents a regularization term that determines the balance between minimal loss and maximal margins. The cost function in Eqs. (9) is solved using Lagrange's formula (Balasundaram and Tanveer, 2013) to obtain the optimized function:

$$f(X) = \sum_{i=1}^{n} (\alpha_i - \hat{\alpha}_i) \phi(X_i, X_j) + b, \tag{10}$$

where, $\alpha_i, \hat{\alpha}_i$ are Lagrange multipliers, and $\phi(X_i, X_j)$ is the kernel function which implicitly maps the training vectors in Eqs. (8) into a higher dimensional space. The SVR method of the *pyESD* package includes linear, polynomial, sigmoid, and Gaussian radial basis functions (RBF) kernels (Hofmann et al., 2008). Moreover, the degree of regularization (C) and the coefficient of the kernels (*gamma*) is given a range of values, so that the hyperparameter optimization algorithm can determine the best model. Due to the expensive nature of SVR, the package uses a randomized search algorithm in a CV setting for the hyperparameters optimization (Bergstra and Bengio, 2012). However, hyperparameters optimization algorithms, such as Bayesian and grid search (Snoek et al., 2012; Pontes et al., 2016; Bergstra et al., 2011) methods, are also provided as alternatives. Previous downscaling projects have taken advantage of the SVR method due to its ability to map data into higher dimensional space and exclude outliers from the training process (Ghosh and Mujumdar, 2008; Chen et al., 2010; Sachindra et al., 2018; Anandhi et al., 2008; Tripathi et al., 2006).

2.3.5 Ensemble Machine Learning

Each ML technique is associated with challenges that arise from the method's limitations and underlying assumptions. These have to be considered carefully in the evaluation of the resulting downscaling product. Some of these challenges can be overcome by an integration of different ML models for a specific task (Dietterich, 2000; Zhang and Ma, 2012). Integrated ML models have been suggested to outperform single ML models in downscaling climate information (e.g. Liu et al., 2015). Ensemble models typically use different ML algorithms (base learners) to extract information from the training data, then use a second set of ML algorithms (meta learners) that learn from the first and combine the individual predictions into an ensemble. Ensemble models can be categorized by (a) the selection of base learners, and (b) the method of combining the individual predictions from the base learners. Here, we summarise the more prominent ensemble models that are included in the *pyESD* package.

Bagging

The bagging ensemble models consist of ML algorithms that generate several instances of base learners using random subsets
330 of the training data, and then aggregate the information for the final estimates (Breiman, 1996; Quinlan, 1996). Such algorithms integrate randomization into the learning process and thereby often ensure the reduction of the variance of the individual base learners (e.g., decision trees). Moreover, the bagging techniques constitute a simple way to improve model performance without the need to adapt the underlying base algorithm. Since bagging works well with complex algorithms like decision trees, we also consider tree-based ensembles for the *pyESD* package. More specifically, we include implementations of the
335 Random Forest (*RandomForest*) and Extremely Randomized Tree (*ExtraTree*) methods in addition to classical *Bagging*.

The *RandomForest* algorithm builds multiple independent tree-based learners. The trees can be constructed with the full set of predictors or a random subset. Each tree is constructed from a random sample of the training data in a bootstrapping process (Breiman, 2001). The algorithm uses the remaining training data (i.e. out of bag data) to estimate the error rate and evaluate the model's robustness. In contrast, the *ExtraTree* algorithm considers the discriminative thresholds from each predictor rather
340 than the subset of predictors (Geurts et al., 2006). This usually adds more weight to the variance reduction and slightly improves the model bias. Tree-based ensembles are particularly suitable for establishing a nonlinear relationship between predictors and predictand (e.g. Pang et al., 2017; He et al., 2016).

Boosting

In recent years, boosting models have also been applied for the downscaling of climate information (e.g. Fan et al., 2021;
345 Zhang et al., 2021). Boosting models are meta-estimators that are built sequentially from multiple base learners with the primary objective of reducing the model bias and variance. In principle, the method 'boosts' the weaker base learner (i.e., estimators that perform only slightly better than random guessing) by converting them into strong ones in an iterative process. The technique assumes that the base learning model is distribution-free (Schapire, 1999) and iteratively improves the weaker base learners by applying weights to the training data through the adjustment of the input points with prediction errors from
350 the previous prediction (Schapire, 2003; Schapire and Freund, 2013). There are many boosting algorithms due to the many possible methods of weighting the training data and tuning the weaker base learners. In the pyESD package, we include (1) Adaptive boosting (Adaboot), (2) Gradient Tree Boosting (GradientBoost) with a gradient boosting algorithm by Friedman (2001), and (3) Extreme Gradient Boosting (XGBoost). A brief summary of each is provided below:

1. The Adaboost algorithm is a well-established model for improving the accuracy of weak base learners (Freund and
355 Schapire, 1997). The model is adaptive in the sense that the training data are sequentially adjusted based on the previous performance of the weaker model. The model uses a weighted majority vote (or sum) to combine the individual prediction from the weaker learners and produce a robust final prediction. The implemented version uses a decision tree algorithm as the base estimator to develop the boosted ensemble predictions.

2. The *GradientBoost* algorithm considers the boosting process as a numerical optimization problem that minimizes a
360 loss function in a stage-wise additive model by adding weaker learners using a gradient descent procedure. This generalization allows the tuning of an arbitrary differentiable loss function which can be selected based on a specific problem. Specifically, in *pyESD*, squared errors are used in the minimization of the loss function.

3. The *XGBoost*, a recent extension of the *GradientBoost* algorithm, is designed to reduce computational time and improve model performance (Chen and Guestrin, 2016). The model uses regularization terms to penalize the final

365 weights and prevent overfitting. The algorithm also uses shrinkage and column subsampling techniques to avoid overfitting. Moreover, the model can handle sparse data by using a sparsity-aware split function.

Stacked Generalization

The Stacked Generalization method (or 'stacking') has previously been used for the downscaling of climate information, and showed improved prediction robustness over singular models (e.g., Massaoudi et al., 2021; Gu et al., 2022). It is designed to

370 enhance prediction accuracy and generality by taking advantage of the mutual complementarity of the base-model predictions. The approach was introduced by Wolpert (1992), and demonstrated for regression tasks and unsupervised learning by Breiman (1996) and Leblanc and Tibshirani (1996), respectively. In principle, the following process is implemented: In the first step, the training data and base models, referred to as level-0 data and level-0 models by Wolpert (1992), are used to generate the first set of predictions. Then a meta-learning model (level-1 generalizer) is used to optimally combine the previous predictions

375 (level-1 data) into final estimates. Lastly, the method applies a cross-validation technique and generates new 'stacked' datasets for a final learning step. Generally, the performance of stacked generalization is constrained by the attributes used to generate the level-1 data, and the type of algorithm used for higher-level learning (Ting and Witten, 1999). We consider these limitations by providing a wide range of models that can be used as the level-0 models and the level-l generalizer. The base-learners can be selected from the different ML models presented in the previous sections. The reader is advised that previous studies (e.g.,

380 Reid and Grudic, 2009) suggest the use of a more restrictive model like *LassoCV* and *ExtraTree* as the meta-learner to prevent overfitting.

2.4 Model training

The process of training and testing the PP-ESD models is the most critical stage in the downscaling procedure, since it determines much of the robustness of the final models, as well as the accuracy of the predictions they generate. The process

385 typically involves the following steps: The observational records are separated into training and testing datasets. The training datasets are used to establish the transfer functions that make up the PP-ESD models. The models are then evaluated on the independent testing datasets (Section 2.5). In the model training process, hyperparameter optimization techniques (e.g., GridSearchCV) are used to fine-tune the transfer function parameters, such as regression coefficients, to optimize model performance. Cross-validation (CV) techniques are applied to split the whole training dataset into smaller training and

390 validation data sections and allow the assessment and iterative improvement of the model parameters during training while also preventing overfitting. In this category of techniques, the k-fold framework is the most used for climate information downscaling models. It partitions the training data into k equally sized and mutually exclusive subsamples, which are also referred to as folds (Stone, 1976; Markatou et al., 2005). More specifically, for each iteration step, one fold is used for model validation, and the remaining k-1 folds are used for model training. The leave-one-out CV technique (Lachenbruch and

395 Mickey, 1968) is an alternative and has been used for the development of ESD models (e.g., Gutiérrez et al., 2013). Cross-

validation techniques rely on the fundamental assumption of independent and identically distributed (i.i.d) data. They, therefore, treat the data as a result of a generative process that has no memory of previously generated samples (Arlot and Celisse, 2010). The assumption of i.i.d might not be valid for time series data (e.g., Bergmeir and Benítez, 2012) due to seasonal effects, for example. To circumvent this problem, monthly-bootstrapped resampling and time-series splitters are included in

400 the *pyESD* package. The *pyESD.splitter* module contains all CV frameworks available for model training, including the k-fold, the leave-one-out, and other CV schemes. The validation metrics used for optimizing the model parameters include the coefficient of determination (R^2) (Eqs. (11)), Root Mean Squared Error (RMSE) (Eqs. (13)), Mean Absolute Error (MAE) (Eqs. (14)), and others that are summarized in Section 2.5. The final values for the validation metrics, which reflect the model performance during training, are arithmetic means of the individual values for each iteration. In this paper, we refer to them as

405 CV performance metrics (i.e., CV R^2, CV RMSE, and CV MAE).

2.5 Model evaluation

In the process of downscaling climate information, best practice involves the use of stringent model evaluation schemes with independent data outside the training data range (Wilby et al., 2004). Retaining a section of the data as a testing dataset (Section 2.4) is recommended if longer records (e.g., ≥ 30 years) are available. It allows (a) a completely independent evaluation of the

410 trained model's performance, and (b) an assessment of the sensitivity of the model to the chosen training dataset. In the case of time series, the latter can provide insights into the model's sensitivity to the calibration period and the temporal stationarity of the model's transfer functions. If the records are short (e.g., < 30 years), the CV metrics (Section 2.4) can be used, albeit with caveats, as non-ideal estimates for the model's performance (e.g., Mutz et al., 2021). For the remainder of this section, however, we will assume that longer records and completely independent testing datasets are available.

415 The PP-ESD model is evaluated on the basis of the model's predictions $\hat{y}$ and the observed values y. In *pyESD*, the following performance metrics are implemented:

1. The coefficient of determination (R^2) represents the fraction of the predictand's observed variance that can be explained by the predictors. It can be seen as a measure of how well the model predicts the unseen data (Wilks, 2011). The R^2 for the predicted values $\hat{y}_i$ in relation to the observed data y_i for i=1,..., n samples is defined as:

$$R^2(y, \hat{y}) = 1 - \frac{\sum_{i=1}^{n}(y_i - \hat{y}_i)^2}{\sum_{i=1}^{n}(y_i - \bar{y})^2} \qquad (11)$$

where $\bar{y}$ is the mean of the observed data, $\sum_{i=1}^{n}(y_i - \hat{y}_i)^2$ is the sum of squared residuals (SSR) and $\sum_{i=1}^{n}(y_i - \bar{y})^2$ is the total sum of squares (SST). R^2 can range from $-\infty$ to 1, where 1 is the best possible score and negative values are indicative of an arbitrary, worse model. An R^2 value of 0 is indicative of a model that would always predict the $\bar{y}$. In this case, the model represents no improvement over simply using the mean $\bar{y}$ as a model.

425 2. Pearson's correlation coefficient (PCC) evaluates the linear correlation between the model predictions y_i and observed data x_i. The PCC of 1 indicates a perfect positive correlation, -1 indicates a perfect anti-correlation, and 0 indicates no correlation between the predicted and observed values. The PCC for n samples is defined as:

$$PCC_{xy} = \frac{\sum_{i=1}^{n}(x_i - \bar{x})(y_i - \bar{y})}{\sqrt{\sum_{i=1}^{n}(x_i - \bar{x})^2}\sqrt{\sum_{i=1}^{n}(y_i - \bar{y})^2}} \tag{12}$$

where the $\bar{x}$ and $\bar{y}$ are the means of the x_i and x_i values respectively.

3. The root mean squared error (RMSE) estimates the mean magnitude of error between the predictions and observations. The RMSE is given in the physical units of the observed data and not standardized. Smaller values indicate better model performance. The RMSE for predictions $\hat{y}_i$ and observations y_i of n samples is calculated as:

$$RMSE(y, \hat{y}) = \sqrt{\frac{1}{n}\sum_{i=1}^{n}(\hat{y}_i - y_i)^2} \tag{13}$$

4. The mean absolute error (MAE) is a scale-dependent accuracy measure that also provides information on the errors between the predictions and observed. The MAE is estimated as the sum of absolute errors normalized by the sample size (n). The MAE is calculated as:

$$MAE(y, \hat{y}) = \frac{1}{n}\sum_{i=1}^{n}(\hat{y}_i - y_i)^2 \tag{14}$$

2.6 GCM-ESD coupling and local-scale predictions

The developed and tested PP-ESD model can finally be coupled to coarse-scale climate information. If the PP-ESD model was developed with the intention to downscale predictions of future climate change, the next logical step is to couple it to GCM simulations forced with different greenhouse gas concentration scenarios. Since PP-ESD is the bias-free downscaling alternative to MOS-ESD, PP-ESD models may be coupled to all GCMs, provided that the predictors are adequately represented by the GCMs. This condition may be alleviated to an extent by standardizing the simulated predictor (Bedia et al., 2020). An analysis of the distribution similarity between the observed and simulated predictors can be conducted to test the assumption of representation. For example, the Kolmogorov-Smirnov (KS) test, which is implemented as part of the *pyESD* package utilities, is a non-parametric statistical hypothesis test that can be used to evaluate the null hypothesis (H_0) that the observation-based predictors and simulated predictors are of the same theoretical distribution.

The first step in ESD-GCM coupling is to utilize the GCM output to recreate the predictors used in the training of the ESD model. This may involve anything from constructing simple temperature regional means to reconstructing multivariate indices for more complex climate phenomena. In the case of index-based predictors such as NAO, EA, SCAN, and others, the simulated indices are reconstructed by projecting the pressure anomalies of the GCM onto the EOF loading patterns of the predictors (e.g., Mutz et al., 2015). This ensures that the physical meaning of the index values is maintained. The ESD model then takes these simulated predictors as input and generates local-scale predictions according to the model's transfer functions. The added value of the resulting downscaling product can be evaluated by comparing the downscaled values to the raw outputs of different GCMs and RCMs. Finally, the high-resolution local-scale predictions can be used to drive climate change impact

assessment models to predict flood frequency (e.g., Padulano et al., 2021; Hodgkins et al., 2017), agricultural changes (e.g., Mearns et al., 1996), changes in water resources (e.g., Dau et al., 2021), and more.

3 Illustrative case study: Neckar Catchment

We demonstrate the complete downscaling workflow and highlight most of the functionalities of the *pyESD* package in an
460   illustrative case study. The study uses the PP-ESD approach and is set in the Neckar catchment, a hydrological catchment in Southwestern Germany that consists of complex mountainous terrain with topographic elevations between 200 to 1000 m above sea level (Fig. 2). The region is climatically complex, since local climates are influenced by atmospheric teleconnection patterns (e.g., NAO, EA, and SCAND), orographic effects (e.g., Kunstmann et al., 2004), and the Mediterranean climate (Bárdossy, 2010; Ludwig et al., 2003). The catchment experiences maximum precipitation (80 - 120 mm/month) and
465   temperature (15 - 18 °C) in the summer months (Fig. 3). The catchment serves as a water supply for drinking and agricultural activities (Selle et al., 2013). We use this catchment for our case study, because (a) it is a suitable region to test the strengths and limitations of the *pyESD* downscaling package, and (b) generating 21st century climate change estimates can contribute to regional climate impact assessments and adaptation.
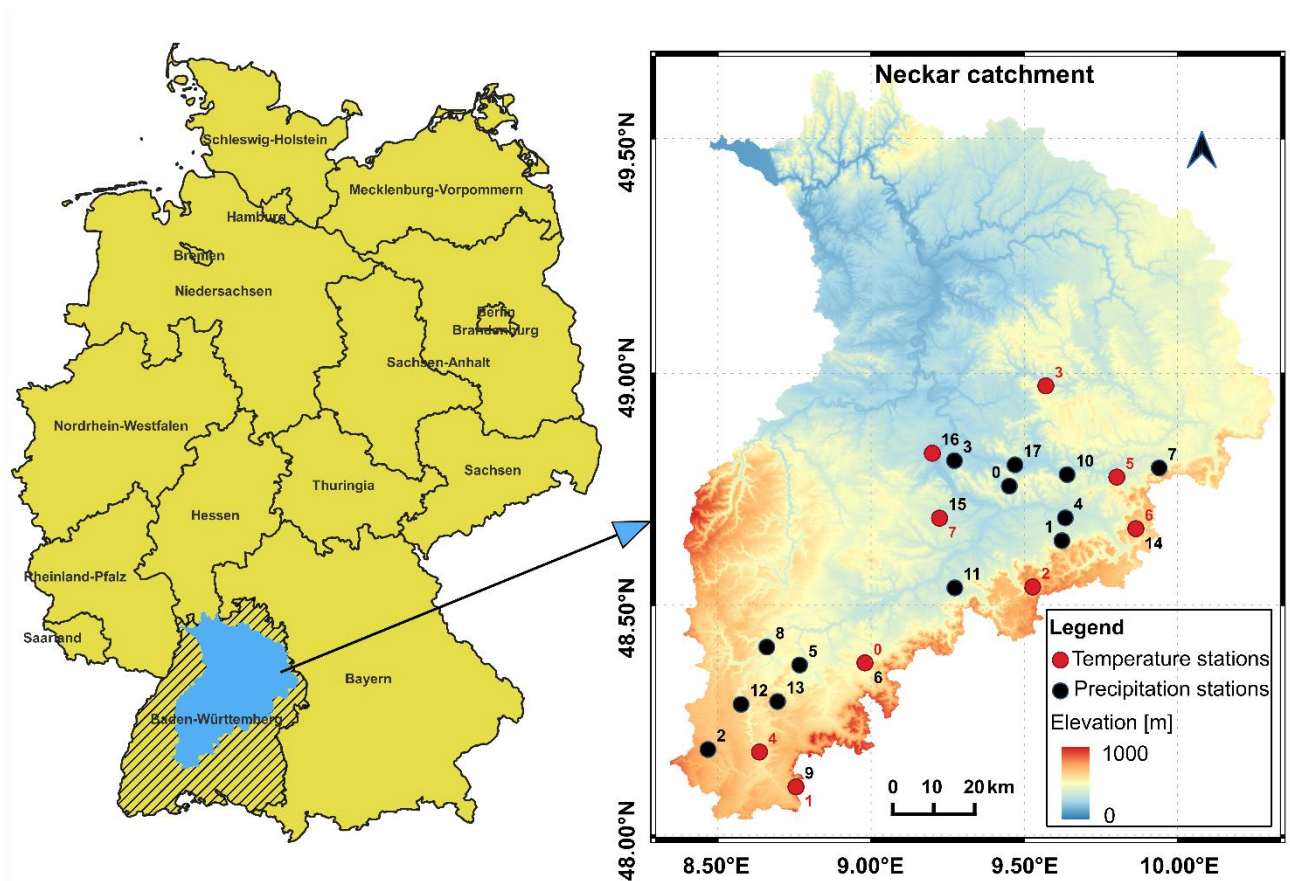
Fig. 2: **Weather station locations and elevations in the Neckar catchment. The red circles represent temperature stations (ID corresponds to Table 1b) and the black circles represent precipitation stations (ID corresponds to Table 1a). The colormap shows the elevation and delineates the extent of the catchment.**
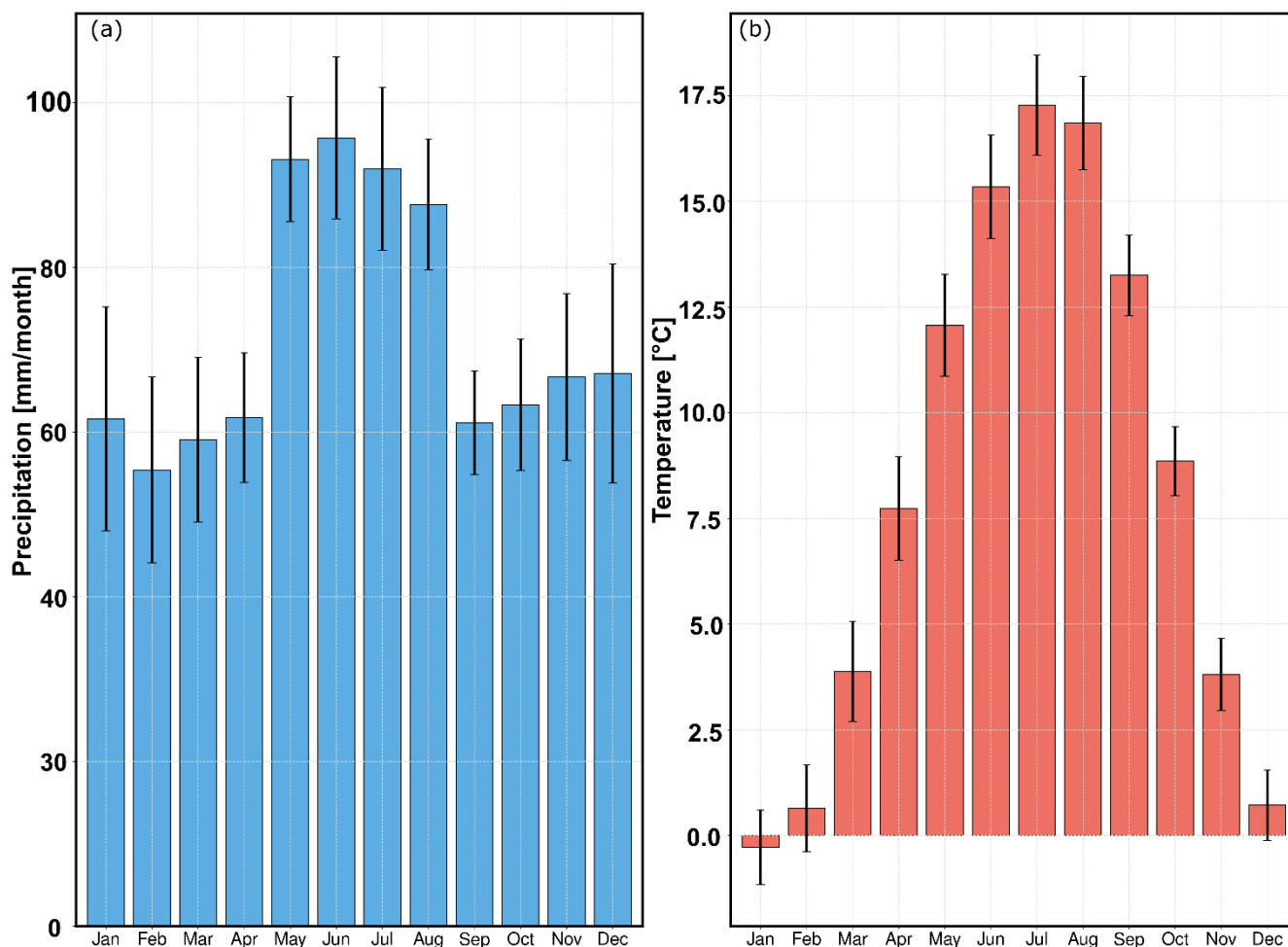
Fig. 3: Long-term (1958 - 2020) monthly means of (a) precipitation and (b) temperature, averaged over all stations in the catchment.
475 **The error bars are the standard deviations that represent inter-station variability. The maximum precipitation and temperature in the catchment are recorded in the summer season (JJA).**

In this case study, we apply *pyESD* to predict local temperature and precipitation changes for 22 weather stations located in the catchment (Table 1), and demonstrate the package's flexibility by performing experiments with the different modeling alternatives. We show most of the PP-ESD steps required for generating robust downscaling products. These steps include (1)

480 predictor selection and construction, (2) model selection, training, and cross-validation, (3) model evaluation, and (4) generating future predictions through ESD-GCM coupling (see Section 3.2 for details). We note that the focus of the case study lies more on demonstrating the *pyESD* workflow and functionality, and less on detailed discussions of the downscaled results and their implications. In order to allow readers to reproduce and learn from this application example, we only use public and freely available datasets (see Section 3.1 for more details about the data). Moreover, all scripts used in this study

485 (i.e. data preprocessing, modeling and visualization scripts) are provided in the supporting material.

Table 1: IDs (specific to this study), names, coordinates and elevation (m) for weather stations recording (a) precipitation and (b) temperature.

ID (a)	Name	Longitude	Latitude	Elevation
1	Baltmannsweiler-Hohengehren	9.45	48.76	457
2	Boll Bad	9.62	48.64	423
3	Eschbronn-Mariazell	8.47	48.19	716
4	Fellbach	9.27	48.81	280
5	Goeppingen-Jebenhausen	9.63	48.69	368
6	Haigerloch-Weildorf	8.77	48.37	524
7	Hechingen	8.98	48.38	518
8	Heubach Ostalb	9.94	48.80	450
9	Horb-Betra	8.66	48.41	544
10	Klippeneck	8.75	48.11	973
11	Lorch Kreis Ostalb-Waldhausen	9.64	48.78	296
12	Metzingen	9.27	48.54	354
13	Oberndorf Neckar	8.58	48.29	516
14	Rosenfeld-Bickelsberg	8.69	48.29	676
15	Stoetten	9.86	48.67	734
16	Stuttgart-Echterdingen	9.22	48.69	371
17	Stuttgart (Schnarrenberg)	9.20	48.83	314
18	Winterbach Rems-Murr-Kreis	9.47	48.80	240
ID (b)	Name	Longitude	Latitude	Elevation
1	Hechingen	8.98	48.38	518
2	Klippeneck	8.75	48.11	973
3	Lenningen-Schopfloch	9.53	48.54	758
4	Murrhardt	9.57	48.97	344
5	Rottweil	8.64	48.18	588
6	Schwaebisch Gmuend-Strassdorf	9.80	48.78	415
7	Stoetten	9.86	48.67	734
8	Stuttgart-Echterdingen	9.22	48.69	371
9	Stuttgart (Schnarrenberg)	9.20	48.83	314

3.1 Datasets

3.1.1 Weather station data

Monthly precipitation and temperature stations data from the German Weather Service (Deutscher Wetterdienst, DWD accessible from https://cdc.dwd.de/portal/) served as the predictand time series in this study. We considered all weather station records that (a) originated from measurements in the Quelle-Enz sub-catchment, (b) covered the time period of 1958 to 2020, and (c) were at least 30a in length. Even though there is no well-established and universally valid recommendation for the minimum record length in an PP-ESD approach (e.g., Hewitson et al., 2014), we chose a conservative 30a threshold to ensure the models can be evaluated with truly independent, retained data (see Section 2.5). The remaining weather stations are summarised in Table 1. These were loaded into predictand Station Objects (SO) as follows:

from pyESD.Weatherstation import read_station_csv

variable = "Temperature" or "Precipitation"

SO = read_station_csv(filename, variable)

3.1.2 Reanalysis datasets

The ERA5 reanalyses products, produced and managed by the European Centre for Medium-Range Weather Forecasting (ECMWF), were used to construct the predictors in this study. ERA5 is based on historical records from various observational systems (e.g., oceans buoys, aircraft, weather stations) that are dynamically interpolated with numerical forecasting models in a four-dimensional variational (4D-Var) data assimilation scheme to generate global, homogeneous, spatially gridded datasets (Bell et al., 2021). It has a spatial resolution of approximately 31 km (or TL639) and is available as hourly data, covering 1950 to the present day (Hersbach et al., 2020). For this study, however, mean monthly values were used in the construction of potential predictors (Table 2). These are publicly available from the Copernicus Climate Data Store (CDS) (accessible at https://cds.climate.copernicus.eu).

Table 2: Potential predictors considered for PP-ESD models and the frequency of their selection for (a) precipitation and (b) temperature stations (based on the final predictor selection method).

	Name	**Description**	**(a)**	**(b)**
1	t2m	Near-surface temperature	8	8
2	tp	Total precipitation	18	9
3	msl	Mean sea level pressure	4	6
4	v10	Near-surface meridional wind	7	7
5	u10	Near-surface zonal wind	10	7
6	NAO	North Atlantic Oscillation Index	9	5

7	EAWR	East Atlantic/Western Russian Oscillation Index	11	3
8	SCAN	Scandinavian Oscillation patterns	11	5
9	EA	East Atlantic patterns	10	4
10	v_plev	Meridional wind at pressure levels 250, 500, 700, 850, and 1000 (hPa	9, 7, 7, 10, 8	7, 3, 8, 5, 7
11	u_plev	Zonal wind at pressure levels 250, 500, 700, 850, and 1000 hPa	4, 9, 7, 6, 11	7, 5, 5, 5, 8
12	r_plev	Relative humidity at pressure levels 250, 500, 700, 850, and 1000 hPa	7, 8, 15, 7, 11	7, 4, 5, 5, 6
13	z_plev	Geopotential height at pressure levels 250, 500, 700, 850, and 1000 hPa	3, 6, 4, 6, 5	4, 6, 5, 7, 5
14	t_plev	Temperature at pressure levels 250, 500, 700, 850, and 1000 hPa	10, 9, 7, 7, 6	5, 5, 6, 8, 9
15	d2m	Near-surface dew-point temperature	6	5
16	dtp	Dewpoint temperature depression	7, 6, 13, 7, 11	4, 2, 2, 3, 1

3.1.3 GCM simulations datasets

515 For the ESD-GCM coupling, the predictors were reconstructed from an MPI-ESM (Max Planck Institute (MPI) Earth System Model (ESM)) GCM simulation that follows the protocols of the World Climate Research Programme's (WCRP) Coupled Model Intercomparison Project phase 5 (CMIP5) (Taylor et al. 2012). For the case study, we consider several simulations (accessible at https://cds.climate.copernicus.eu) forced with different RCPs scenarios (Moss et al. 2010) to predict the local-scale response to the plausible range of forcings. In order to highlight the added value of the downscaled product, the local-

520 scale future estimates are compared to the coarser predictions of several GCMs (i.e., MPI-ESM, CESM1-CAM5 of the National Center for Atmospheric Research (NCAR) (Kay et al., 2015) and HadGE2-ES of the Hadley Centre of the UK Met Office (Collins et al., 2008)) and RCMs (CORDEX-Europe simulation with MPI-CSC-REMO2009 driven with boundary conditions from MPI-ESM).

3.2 Methods

525 **3.2.1 Predictor selection and construction**

The considered predictors must be large-scale climate elements that are both physically and empirically relevant to predicting the local-scale climate variability in the vicinity of the weather station. The physical relevance of considered predictors (Table 2) is established through previous studies and general climatological merit. We then apply a monthly standardizer transformer to remove the seasonality trends and scale the individual predictors. The empirical relationship with the predictand is then

530 evaluated with PCCs defined in Eqs. (12). Finally, first estimates of their predictive skills are obtained through the application of the package's Recursive, Sequential, and TreeBased algorithms in a CV setting. These preliminary experiments are

conducted to refine the selection of predictors further. After the predictor selection process, each weather station and predictand is associated with a particular subset of predictors (Table 2) that are later used to train the final ESD model for the station (Section 3.2.2).

535 The steps above are implemented with *pyESD* as follows:

1. We create a list (*predictors*) of all considered predictors with physical relevance to the predictand. We then use the *set_predictors* method of the station object (*SO*) to read the data in the local directory (*predictordir*) and construct regional means with a defined radius of 200 km around the station location. These are regional means of relevant climate variables and serve as the simplest type of predictor. For the construction of indices for atmospheric

540 teleconnection patterns (i.e., NAO, EA, SCAN, and EAWR), which serve as further predictors, the package automatically calls *pyESD.teleconnections* module if the pattern's acronym is included in the list of predictors.

   predictors = ["t2m", "tp", "NAO", ..., "nth predictor"]

   SO.set_predictors(variable, predictors, predictordir, radius=200) # radius in km

545

2. We apply the monthly standardizer and then use the *predictor_correlation* method to estimate the PCC between the predictand and predictors.

   SO.set_standardizer(variable, standardizer = MonthlyStandardizer(detrending=True, scaling=True))

   df_corr = SO.predictor_correlation(variable, predictor_range, ERA5Data, fit_predictors=True,

550 *fit_predictand=True, method="pearson")*

3. The final refinement of the predictor list is implemented as part of the *fit* method. We use the *set_model* method to define the *ARD* regressor, *TimeSeriesSplitter* CV setting, and call the *fit* method in a loop through the three types of

555 selector methods.

   SO.set_model(variable, method="ARD", cv=TimeSeriesSplit(n_splits=10))

   selector_methods = ["Recursive", "TreeBased", "Sequential"]

   for selector_method in selector_methods:

   SO.fit(variable, predictor_range, ERA5Data, fit_predictors=True, predictor_selector=True, selector_method =

560 *selector_method, select_regressor)*

3.2.2 Model training and validation

Model training and validation is performed separately for each predictand and weather station. The models are trained in a CV setting for the period 1958-2010, and then assessed on independent retained data for the period 2011-2020. In the training

process, we use 7 different methods before deciding on an estimator for the final model. These methods include at least one

565 representative for each of the families of ML algorithms (see section 2.3) except SVR. We exclude SVR due to its high computational demands for optimization, and to ensure the easy reproducibility of the illustrative example on less powerful computers. We perform the initial model training and validation with the *LassoLarsCV, ARD, MLP, RandomForest, XGBoost, Bagging* and *Stacking* regressors using a *KFold(n_splits=10)* validation scheme for hyperparameter optimization. For the *Stacking* regressor, we use all the other regressors as base estimators (i.e., level-0 learners) and *ExtraTree* as the meta-learner.

570 The final ESD model is then selected based on the CV metrics (i.e., CV R² and CV RMSE) of the individual models.

The steps above are implemented with *pyESD* as follows: The models are trained with the *fit* method as described in Section 3.2.2. The *cross_validate_and_predict* method is applied to calculate the CV metrics and generate the predictions for the training period 1958-2010. The *predict* method is then used to generate predictions for the 2011-2020 period from the models trained in the 1958-2010 period. Finally, the *evaluate* method is used to obtain the model performance metrics based on the

575 2011-2020 predictions and retained data. The R², RMSE, and MAE (see section 2.5) are used as both CV and evaluation metrics in this study. The ERA5 reanalysis product is specified as the predictor dataset for all these methods.

cv_score_1958to2010, predict_1958to2010 = SO.cross_validate_and_predict(variable, from1958to2010, ERA5Data)

predict_2011to2020 = SO.predict(variable, from2011to2020, ERA5Data)

580 *scores_2011to2020 = SO.evaluate(variable, from2011to2020, ERA5Data)*

3.2.3 Future prediction

Future predictions are generated by coupling the final ESD models to GCM simulations for the 21st century. In the illustrative example, we use MPI-ESM simulations that were forced with greenhouse gas concentration scenarios RCP2.6, RCP4.5 and RCP8.5. This coupling is achieved as follows: The predictors selected during model training are reconstructed from the GCM

585 output. These simulated predictors are standardized with the *MonthlyStandardizer* parameters obtained from the reanalysis predictors to ensure data homogenization. Prediction anomalies are calculated using the training period 1958-2010 as a reference. The resulting, RCP-specific 21st century prediction anomaly time series are then used to calculate the annual means (2020-2100), as well as the seasonal (DJF, MAM, JJA, SON) and annual 30a climatologies for the mid-century (2040-2070) and the end of the century (2070-2100). The predicted anomalies are then back-transformed to their respective absolute values

590 for all stations and compared to the raw outputs of GCMs (i.e., CESM1-CAM5, HadGE2-ES, EURO-CORDEX, and MPI-ESM; see Section 3.1.3) using the nearest grid point. In *pyESD*, a future prediction can be generated by using the *predict* method (Section 3.2.2) and specifying the GCM output as the predictor data source.

The PP-ESD approach relies on the assumption that the predictors are well represented by the GCM. We therefore perform KS tests to evaluate the distribution similarity between GCM and ERA5 predictors for the datasets' temporal overlap. We

595 perform the test on the raw monthly time series, monthly anomalies and standardized anomalies in order to isolate the distributional differences of the first and second moments error propagation (Bedia et al., 2020). The *KS_stat* function

implemented in the *pyESD.utils* module is used to test several of the informative predictors (such as tp, t2m, r850, u850, and v850).

4.0 Results and Discussion

600 In this section, we present and discuss the results of the illustrative case study. The discussion places more emphasis on the functionalities of the package than the climatological implications. Specifically, we discuss the results of the predictor selection step (Section 4.1), the training and validation of the model (Section 4.2), the final model performance (Section 4.3), and the future predictions generated through the ESD-GCM coupling (Section 4.4).

4.1 Predictor selection

605 All implemented predictor selection methods demonstrated merit, and the correlation analyses revealed strong linear dependencies between the predictand variables and potential predictors (Fig. A1 and A2). For example, precipitation records are highly correlated (PCC $\geq$ 0.5) with large-scale total precipitation (tp), atmospheric relative humidity (r), and zonal winds velocity (u) up to mid-tropospheric level (i.e., 500 - 1000 hPa) (Fig. A1). The temperature records are highly correlated (PPC $\geq$ 0.7) with near-surface temperature (t2m), atmospheric temperature (t on all levels), and dewpoint temperature depression

610 (dtp) up to the mid-troposphere (Fig. A2). Both predictands also show a good correlation (PCC $\geq$ 0.25) with the indices of the atmospheric teleconnection patterns (i.e., NAO, EA, EAWR, and SCAN). The predictor selection methods (i.e., *Recursive*, *TreeBased*, and *Sequential*) perform similarly for all the precipitation and temperature stations (Fig. 4). More specifically, the three methods yield CV R² values of 0.5 to 0.75 (Fig. 4a), CV RMSE values of $\leq$ 25 mm/month (Fig. 4c) for precipitation, CV R² values of $\geq$ 0.95 (Fig. 4b), and CV RMSE values of 0.3 to 0.6 °C (Fig. 4d) for temperature stations. Since the methods did

615 not show a significant difference in performance, the *Recursive* method was applied for the refinement of the set of predictors, since it allows more flexibility and a stepwise iteration of several combinations of potential predictors (e.g., Mutz et al., 2021; Hammami et al., 2012; Li et al., 2020). The frequencies with which specific predictors were selected using the *Recursive* method are listed in Table 2.
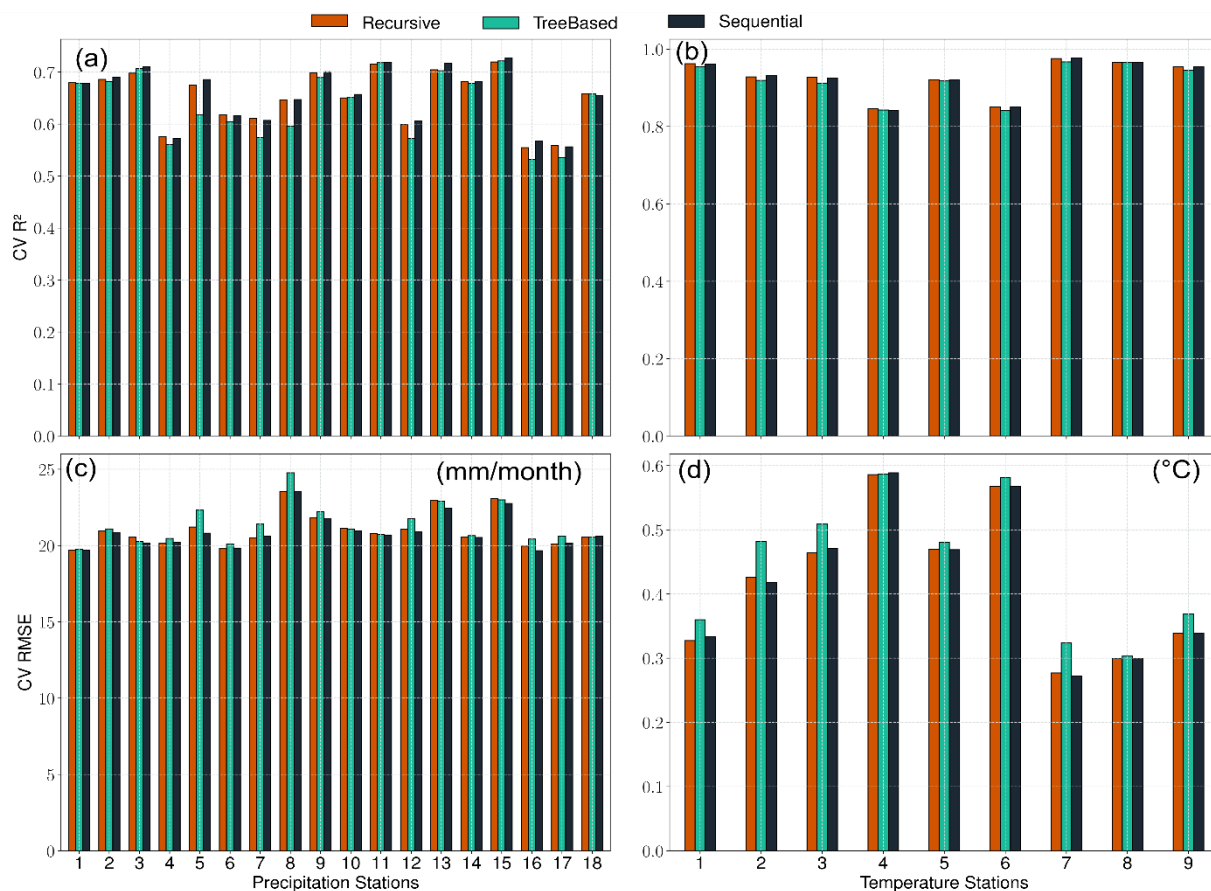
Fig. 4: Cross-validation R² and RMSE for the predictor selection methods (*Recursive* (red), *Tree-based* (green), and *Sequential* (black)) for precipitation (a, c) and temperature (b, d) station records. The individual performed similarly well, suggesting that each of the implemented methods may be used to refine the list of potential predictors.

The predictors tp and t2m were included for most of the precipitation and temperature station records, respectively. This indicates that variations in the larger-scale precipitation and temperature fields already explain much of the local-scale predictand variability in the vicinity of the weather stations. Many of the refined predictor sets also included indices of the NAO (9/18 precipitation stations, 5/9 temperature stations), SCAN (11/18 precipitation stations, 5/9 temperature stations), EA (10/18 precipitation stations, 4/9 temperature stations), and EAWR (11/18 precipitation stations, 3/9 temperature stations). This confirms the strong manifestation of Northern hemisphere atmospheric teleconnection patterns on the local-scale precipitation and temperature in the catchment (e.g., Bárdossy, 2010; Ludwig et al., 2003). Their exclusion from the other stations is likely due to the fact that their variability might already be captured by zonal and meridional wind speeds and synoptic pressure variables like geopotential height (z) and mean sea level pressure (slp) (Hurrell and Van Loon, 1997; Hurrell, 1995; Barnston and Livezey, 1987; Maraun and Widmann, 2018). Relative humidity was selected as a predictor for most of

the precipitation stations. This is consistent with the results of many other studies (e.g., Gutiérrez et al., 2019; Hammami et al., 2012) and our physical understanding of it as a measure of humidity that takes saturation vapor pressure into consideration.

4.2 Performance of individual estimators

We experimented with seven different regressors before deciding on the regressor that would be used to establish the final ESD models (see section 3.2.2). A total of 126 precipitation and 63 temperature experimental models were generated with the seven regressors. Overall, most of the experimental models performed reasonably well with a mean CV R² of ≥ 0.5 for precipitation and ≥ 0.9 for temperature stations (Fig. 5). The MLP models, on the other hand, performed relatively poorly with CV R² values of ≤ 0.4 for precipitation and ≤ 0.9 for temperature. This is due to the fact that MLP model calibration requires longer records and a more complex architecture to capture most of the informative patterns in the training data. This study, however, uses a simplified architecture to make the results reproducible without higher computational requirements. The result can likely be improved with more data (e.g., by using daily values) and an increase in hidden layers (Section 2.2.3). The overall performance of the experimental models underlines the methods' suitability for downscaling.
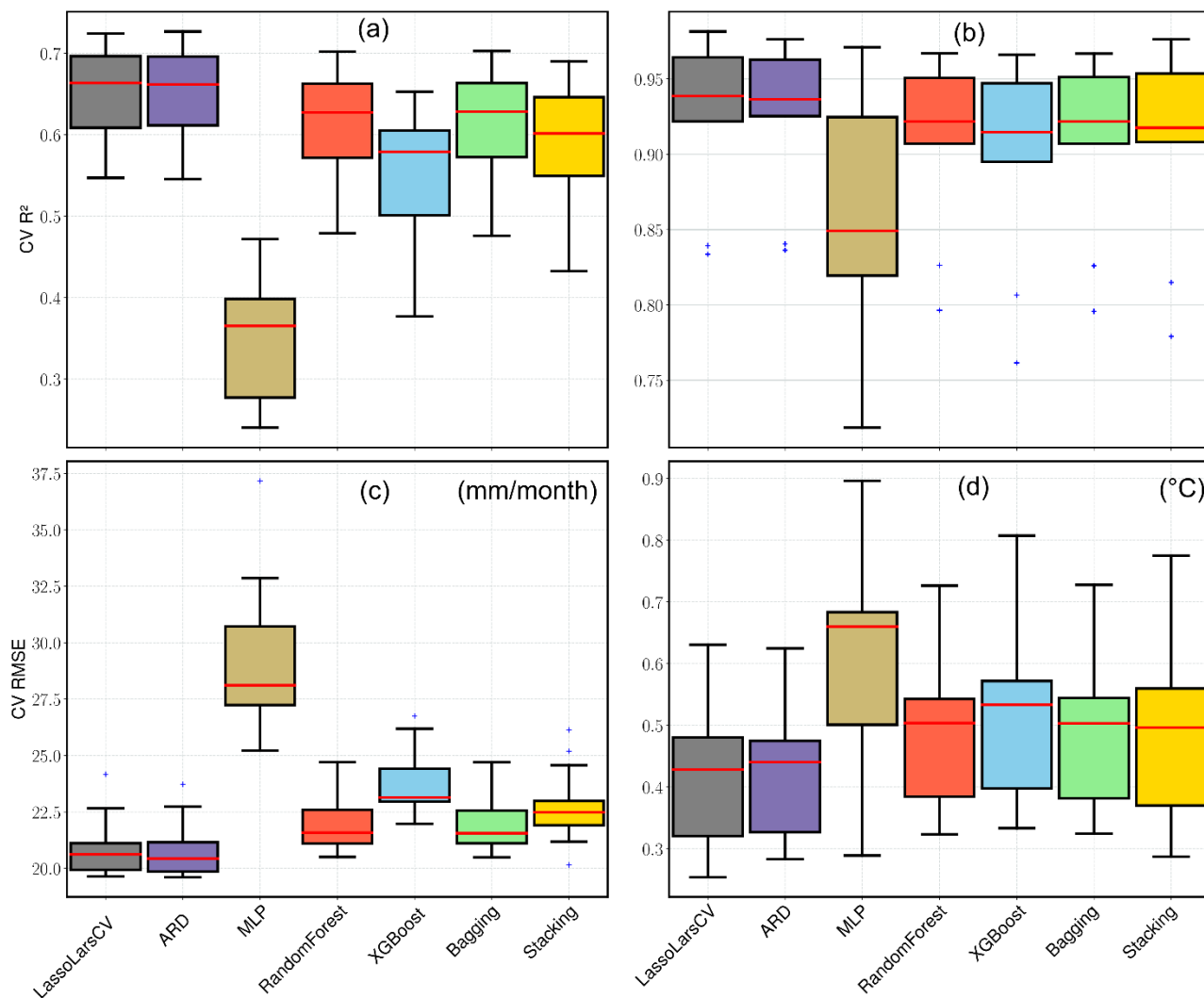
645

Fig. 5: Cross-validation R² and RMSE box plots comparing the experimental regressors' performance for all the precipitation (a, c) and temperature (b, d) stations. The red lines inside the box represent the median, the lower and upper box boundaries indicate the 25th and 75th percentiles, and the lower and upper error lines show the 10th and 90th percentiles, respectively. The black plus marks show the outliers outside the range of the 10th and 90th percentile.

650   Among the better performing precipitation models, the *LassoLarsCV* and *ARD* methods yielded the best results (CV R² = 0.55 - 0.75, CV RSME = 20 - 23 mm/month), followed by the *RandomForest* and *Bagging* ensembles (CV R² = 0.48 - 0.70, CV RSME = 21 to 25 mm/month), and *XGBoost* ensemble regressor (CV R² = 0.39 - 0.65, CV RMSE = 22 - 27 mm/month). Stacking all experimental models into a meta-regressor also yields good results (CV R² = 0.45 - 0.7, CV RMSE = 20 - 26 mm/month) despite the poor performance of the MLP regressors. Based on these results, the *LassoLarsCV*, *ARD*,

655   *RandomForest*, and *Bagging* regressors were selected as the final base learner for the *Stacking* model. *ExtaTree* was chosen

as the final meta-learner to prevent overfitting issues by placing an additional discriminative threshold on all the base regressor's predictions (Geurts et al., 2006).

The experimental temperature models showed similar patterns in performance, but performed better overall. The *LassoLarCV* and *ARD* emerge as the best-performing models (CV R² = 0.85 - 0.98, CV RMSE = 0.2 - 0.6 °C), followed by the

660 *RandomForest* and *Bagging* regressors (CV R² = 0.8 - 0.96, CV RMSE = 0.3 - 0.7 °C), and the *XGBoost* and *Stacking* ensemble regressors (CV R² = 0.75 - 0.96, CV RMSE = 0.3 - 0.8 °C). Therefore, we also selected *Stacking* (with *LassoLarsCV, ARD, RandomForest, Bagging)* for the final temperature models, too.

4.3 Performance of the final estimator

Following the analysis of the seven experimental models (Section 4.2), the *Recursive* predictor selection method and *Stacking*

665 learning model *(with LassoLarsCV, ARD, RandomForest,* and *Bagging)* were selected for the generation of the final ESD models. The models were trained on the 1958-2010 data in a CV setting, and evaluated on the retained data in the 2011-2020 period. R², RMSE, and MAE were used as performance metrics for the CV setting and the final evaluation (Tables 3 and 4). The models' performance was good overall, but varied notably between different stations. The prediction skill estimates were higher for temperature than for precipitation. For temperature (Table 4), the explained variance estimates ("Fit R²") are in the

670 range of 0.81-0.98 (μ=0.94), and CV R² are in the range of 0.84 to 0.98 (μ=0.93), whereas for precipitation (Table 3), the explained variance estimates are in the range of 0.58-0.84 (μ=0.71), and CV R² are in the range of 0.54-0.72 (0.65). The accuracy measures display a similar discrepancy with CV RMSE of 0.3-0.6 °C (μ=0.42 °C) and CV MAE of 0.2-0.50 °C (μ=0.34 °C) for temperature, and CV RMSE of 20-24 mm/month (μ=21 mm/month) and CV MAE of 14-18 mm/month (μ=16 mm/month) for precipitation.

675

Table 3: Model performance metrics (i.e., R², RMSE, and MAE) for all the precipitation stations. The final ESD models were trained in a CV setting on datasets from 1958-2010, and evaluated on independent, retained data from 2011-2020.

ID	Name	(Fit) R²	CV R²	CV RMSE	CV MAE	R²	RMSE	MAE
1	Baltmannsweiler-Hohengehren	0.71	0.67	20	15	0.63	22	18
2	Boll Bad	0.70	0.69	21	15	0.60	24	19
3	Eschbronn-Mariazell	0.74	0.69	20	16	0.59	23	18
4	Fellbach	0.61	0.57	20	15	0.59	20	15
5	Goeppingen-Jebenhausen	0.71	0.68	21	16	0.62	23	18
6	Haigerloch-Weildorf	0.64	0.62	20	15	0.74	17	13
7	Hechingen	0.63	0.61	20	15	0.74	17	13

8	Heubach Ostalb	0.78	0.65	24	18	0.65	25	21
9	Horb-Betra	0.84	0.72	21	16	0.74	21	16
10	Klippeneck	0.67	0.63	21	16	0.70	21	17
11	Lorch Kreis Ostalb-Waldhausen	0.79	0.72	21	15	0.64	24	20
12	Metzingen	0.79	0.61	20	16	0.64	20	16
13	Oberndorf Neckar	0.75	0.71	23	17	0.66	28	22
14	Rosenfeld-Bickelsberg	0.70	0.69	20	15	0.70	21	16
15	Stoetten	0.75	0.72	23	17	0.68	25	20
16	Stuttgart-Echterdingen	0.61	0.56	20	14	0.68	16	13
17	Stuttgart (Schnarrenberg)	0.58	0.54	20	14	0.50	21	15
18	Winterbach Rems-Murr-Kreis	0.72	0.66	20	15	0.61	23	18

Table 4: Model performance metrics (i.e., R^2, RMSE, and MAE) for all the temperature stations. The final ESD models were trained in a CV setting on datasets from 1958-2010, and evaluated on independent, retained data from 2011-2020.

ID	Name	Train R^2	CV R^2	CV RMSE	CV MAE	R^2	RMSE	MAE
1	Hechingen	0.96	0.96	0.30	0.30	0.93	1.3	1.2
2	Klippeneck	0.94	0.94	0.40	0.30	0.94	1.3	1.2
3	Lenningen-Schopfloch	0.95	0.93	0.50	0.40	0.91	0.9	0.7
4	Murrhardt	0.81	0.84	0.60	0.50	0.77	1	0.8
5	Rottweil	0.94	0.92	0.50	0.40	0.92	1.1	1
6	Schwaebisch Gmuend-Strassdorf	0.89	0.85	0.60	0.50	0.91	0.5	0.4
7	Stoetten	0.98	0.98	0.30	0.20	0.94	1.4	1.4
8	Stuttgart-Echterdingen	0.98	0.97	0.30	0.20	0.94	1.5	1.4
9	Stuttgart (Schnarrenberg)	0.98	0.96	0.30	0.30	0.95	1.6	1.5

The final model evaluation using independent, retained data from 2011-2020 yielded R^2 values of up to 0.95, and average RMSE and MAE of ~ 1.0 °C for temperature, and R^2 values of up to 0.74, average RMSE of 22 mm/month, and MAE of 17 mm/month for precipitation. The discrepancy in temperature and precipitation model performance is unsurprising, since the

685   thermodynamics and atmospheric dynamics controlling precipitation variability are more difficult to represent (e.g., Shepherd, 2014). Regardless, the overall performance speaks in favor of applying the study's approach to downscale mid-latitude climate in complex terrain. Moreover, the models' similar performance during CV and the final evaluation indicates that the models were not overfitted, and that the predictand-predictors relationships hold outside the observed period. Finally, it is worth noting that the *Stacking* regressor performed better than the individual base models, even when all the potential regressors of the

690   initial experiments (Section 4.2) were stacked into a meta-regressor. Such improvements demonstrate the advantage of the ease-of-experimentation through a package like *pyESD*.

We visualize a prediction example (Fig. 6) to (a) provide a less abstract presentation of these results, and (b) demonstrate the type of figure generated by the plotting utility functions in the *pyESD.plot* module. The figure depicts the predictions generated by the final ESD model for the Hechingen station. A station that records precipitation and temperature (station ID 7 and 1,

695   respectively). The observed and predicted values for 2011-2020 are highly correlated, with PCCs of 0.85 (Fig. 6a) for precipitation and 0.97 (Fig. 6b) for temperature. The time series comparisons also demonstrate the models' abilities to predict the variability of the observed values in both the training and testing period (Fig. 6 a and b). Prior to this study, PP-ESD models have not been directly applied to the weather stations in the catchment. However, our models are among the best performing for temperature and precipitation when we compare them to models from other studies across Europe (e.g., Gutiérrez et al.,

700   2019; Hertig et al., 2019; Schmidli et al., 2007). For instance, Gutiérrez et al., (2019) performed an intercomparison of statistical downscaling model performance for 86 stations across Europe using the MOS, PP, and WG methods. The Spearman correlation of the downscaled and observed values yielded R values in the range of ~ 0.0 - 0.7 (with many stations ≤ 0.5) for precipitation and 0.3 - 0.95 for temperature. These comparisons also underline the suitability of the *pyESD* methods for downscaling climate information even in complex, mountainous regions.
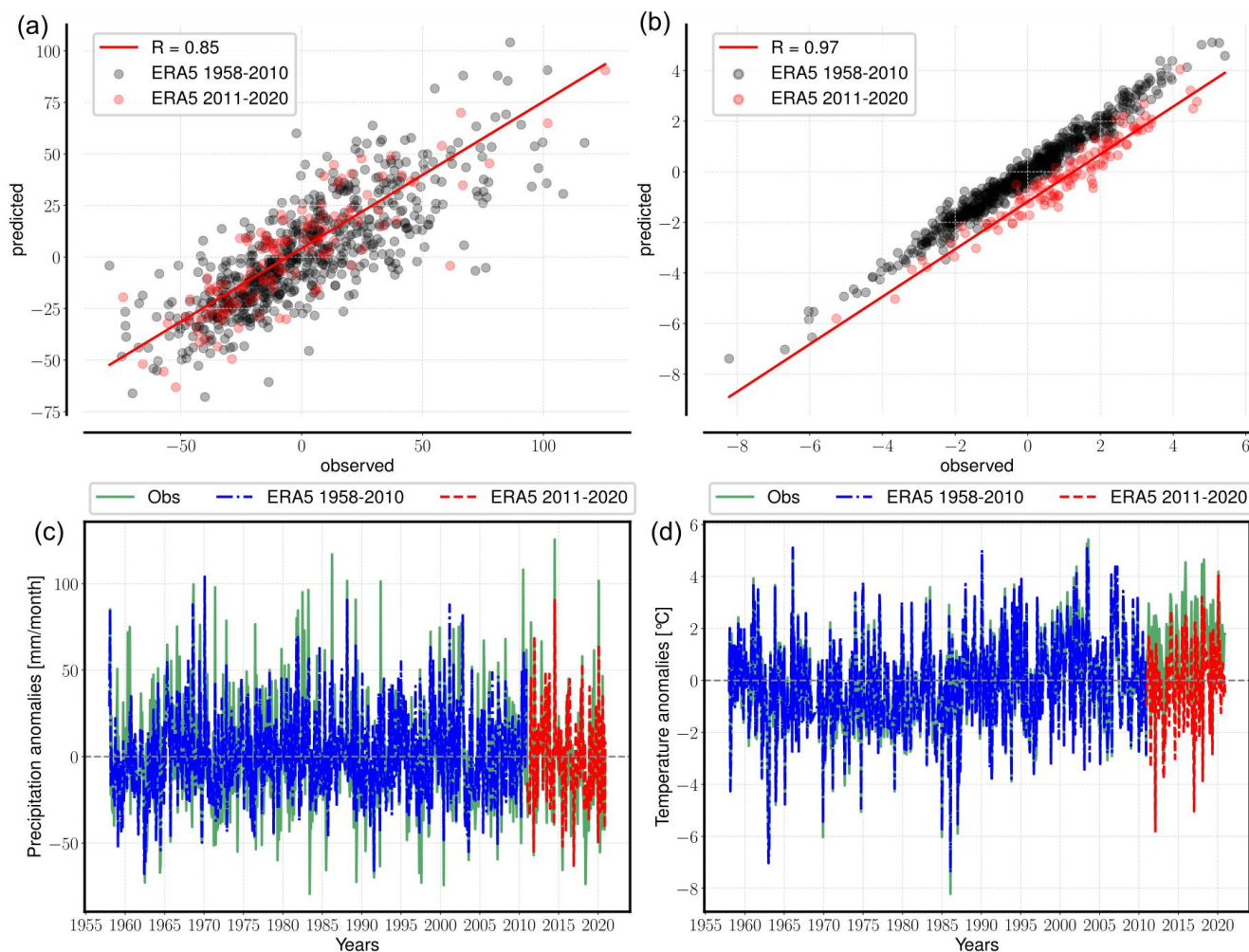
Fig. 6: Prediction example for the Hechingen station using the final regressor for precipitation (a, c) and temperature (b, d). The top panel (a-b) shows the linear relationship between the predictions and observed values, and the PCC (R value) for the testing data (red-colored circles). The bottom panel (c-d) shows the 1-year moving average of the observed (green, solid) and ERA5-driven predictions for the training period (blue, dash-dotted) and the testing period (red, dashed).

710   **4.4 Prediction of local responses to 21st century climate change**

The predictions of local precipitation and temperature responses to 21st century climate change were generated by coupling the final ESD models to MPI-ESM simulations forced with greenhouse gas concentration scenarios RCP 2.6, RCP 4.5, and RCP 8.5 (Section 3.2.3). The results are presented as deviations from the monthly long-term means of the training period (1958 - 2010) and referred to as "anomalies" hereafter. The annual mean anomaly time series were computed with a 1-year moving average with a centered mean (Fig. 7 and 9).
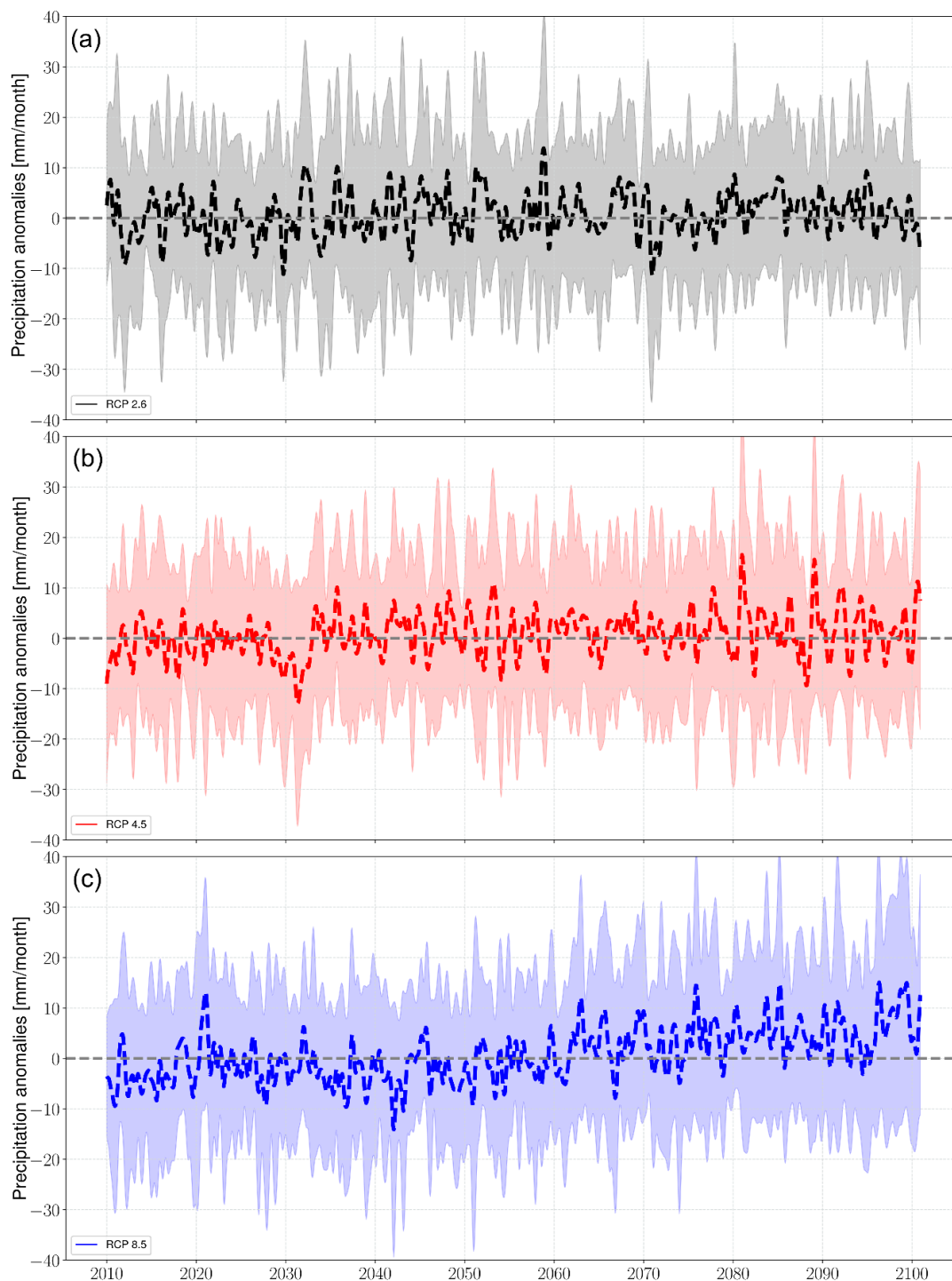
Fig. 7: Predicted regional annual means of the precipitation in response to (a) RCP 2.6 (black), (b) RCP 4.5 (red), and (c) RCP 8.5 (blue). The solid lines represent the values averaged over all stations, and the shaded boundaries indicate the corresponding variability range (one standard deviation). The time series are smoothed with a 1-year moving average with a centered mean.

720 The precipitation predictions (Fig. 7) for RCP 8.5 (RCP 4.5) show a strong (weak) positive trend towards the end of the century. This trend is even more pronounced for the predicted temperatures (Fig. 9) in the catchment. The predicted precipitation changes vary greatly between weather stations. Furthermore, the RCPs change the magnitude, but not the pattern of the predictions for each station. For instance, stations that show an increase (decrease) in precipitation for the RCP 2.6, predict a greater increase (decrease) in response to RCP 4.5 and RCP 8.5. The annual and seasonal 30a end-of-century climatologies

725 show an overall increase in precipitation in response to both RCP 2.6 and RCP 4.5 (Fig. 8) for most of the stations. The annual end-of-century climatologies deviate from the present-day (1958-2010) by ca. -5 to 20 mm/month for RCP 8.5 and ca $\leq$ 5 mm/month for RCP 2.6. Overall, the ESD models predict a precipitation increase of ca. 10 - 20 % until the end of the century. Furthermore, the seasonal climatologies reveal a shift of maximum precipitation away from the summer season for some stations. Such shifts in seasonality and an overall decrease in summer precipitation have previously been predicted (e.g., Gobiet

730 et al., 2014; Paparrizos et al., 2017; Feldmann et al., 2013). Prior to this study, no ESD-GCM based prediction of the 21st century precipitation changes have been developed for the weather stations of the catchment. However, the models' predictions of the precipitation response to higher greenhouse gas concentration scenarios are comparable to coarser predictions by other studies using RCMs or ESD models (Feldmann et al., 2013; Kunstmann et al., 2004; Paparrizos et al., 2017; Lau et al., 2013). The precipitation predictions generated in this case study can be used further for climate impact assessments, such as

735 assessments of the probability of flooding and drought across the hydrological catchment. The projected shifts in seasonality across the catchment represents potentially valuable information for agricultural planning.
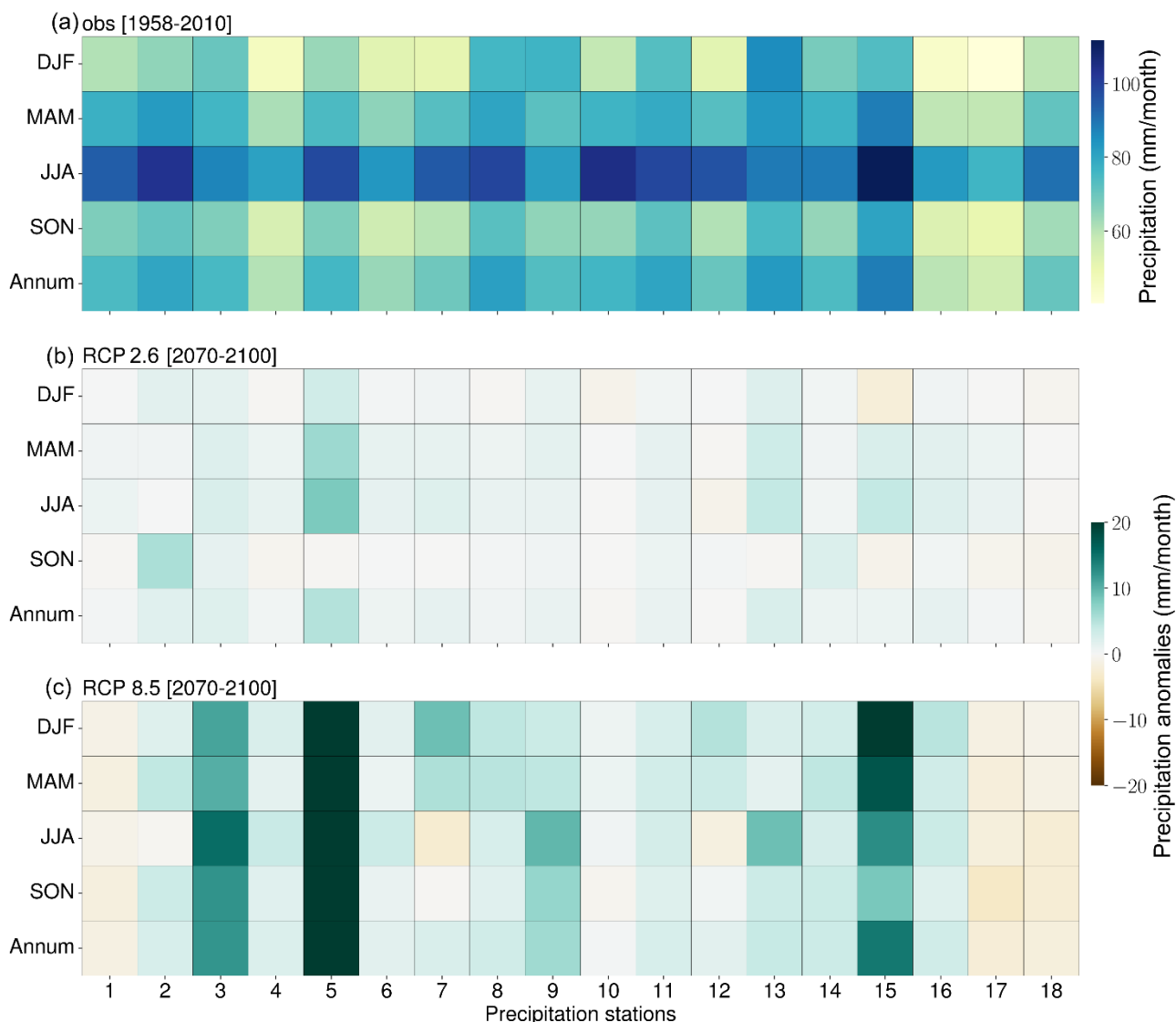
Fig. 8: Observed precipitation (1958-210), and seasonal (i.e., spring (MAM), summer (JJA), autumn (SON), and winter (DJF)) and annual end-of-century (30-year) precipitation climatologies as a result of RCPs 2.6 (b), and RCP 8.5 (c) forcing. The brown (green) colors indicate a decrease (increase) in precipitation relative to the observed means (1958-2010).

The predicted temperature anomalies (Fig. 9) reveal a strong (weak) positive trend for RCP 8.5 (RCP 4.5). The end-of-century climatologies reveal only moderate warming of ca. -0.5 to 1 °C for RCP 2.6, and significant warming (ca. 2 - 4 °C) for all seasons in response to RCP 8.5 (Fig. 10). More specifically, the investigated region is predicted to experience most warming (≥ 3 °C) in the summer season. There are few differences in predicted warming between the stations of the catchment. Generally, the estimated magnitude of warming towards the end of the century is in agreement with the IPCC report (Masson-Delmotte et al., 2021) and other downscaled estimates (e.g., Kunstmann et al., 2004; Gutiérrez et al., 2019). The predicted

warming would likely implicate the societal and ecological systems, and stresses the need for efficient adaptation and mitigation strategies.
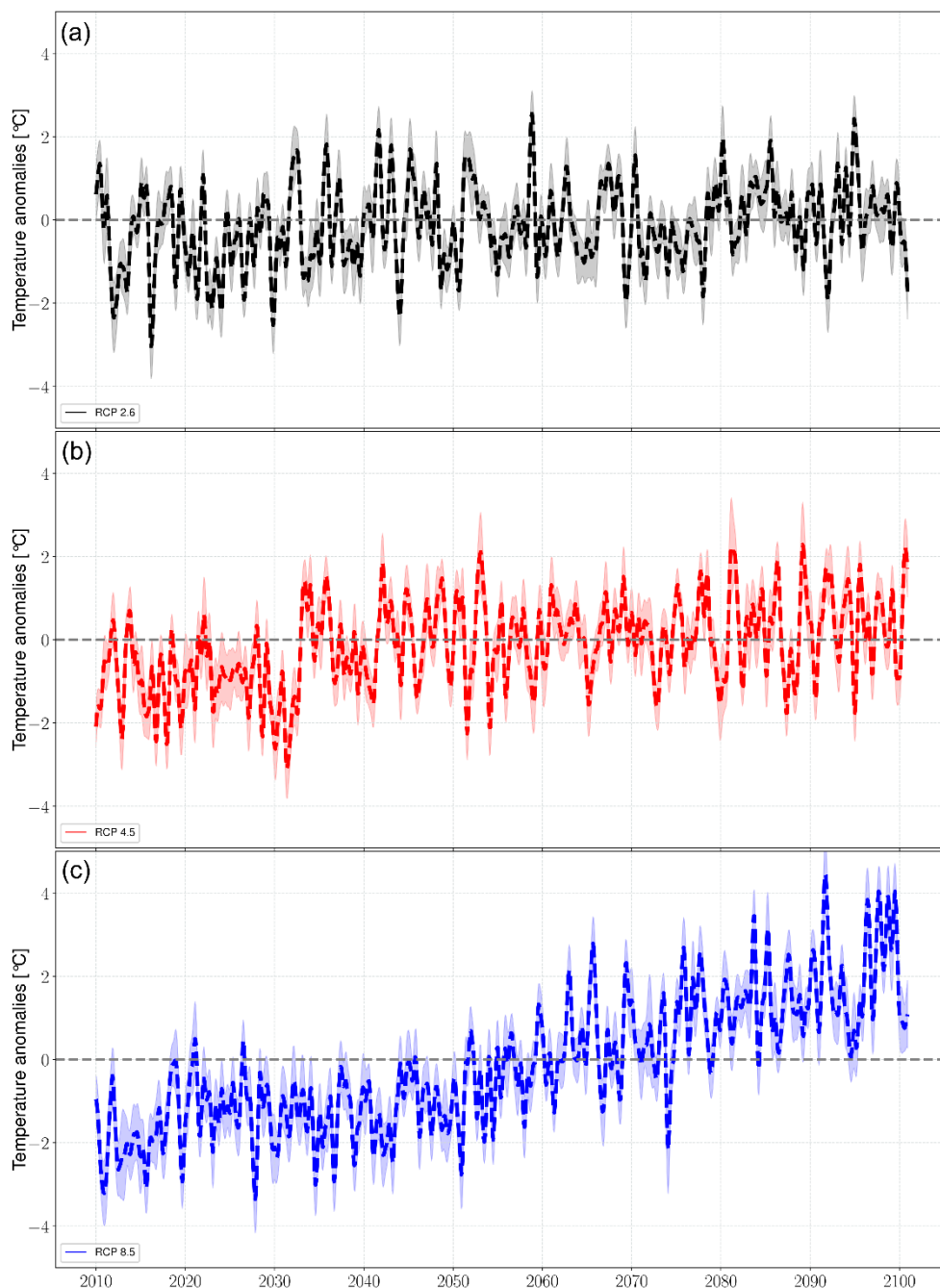
750 **Fig. 9: Predicted regional annual means of the temperature in response to (a) RCP 2.6 (black), (b) RCP 4.5 (red), and (c) RCP 8.5 (blue). The solid lines represent the values averaged over all stations, and the shaded boundaries indicate the corresponding variability range (one standard deviation). The time series are smoothed with a 1-year moving average with a centered mean.**
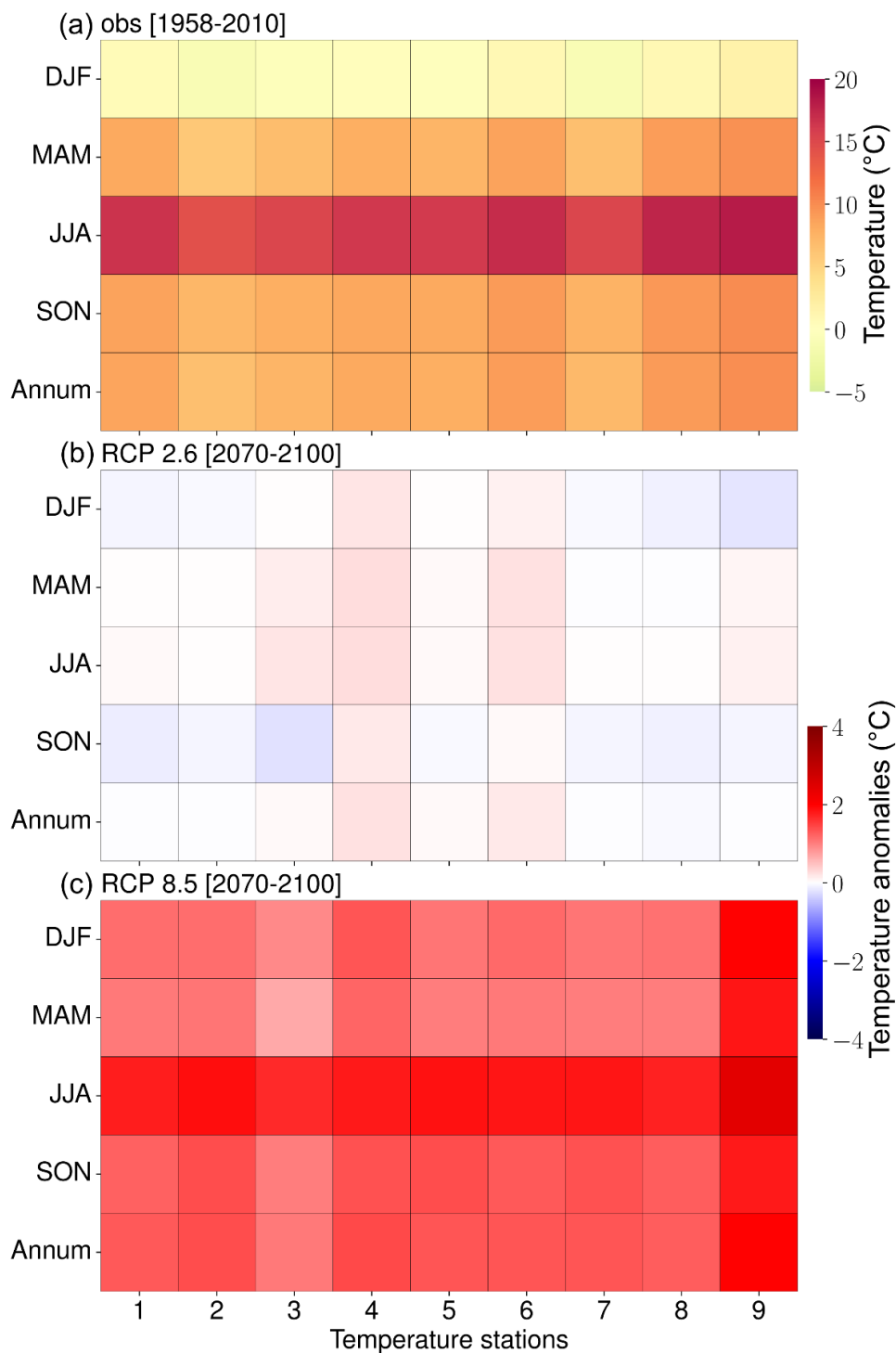
Fig. 10: Observed temperature (1958-210), and seasonal (i.e., spring (MAM), summer (JJA), autumn (SON), and winter (DJF)) and
755   **annual end-of-century (30-year) temperature climatologies as a result of RCPs 2.6 (b), and RCP 8.5 (c) forcing. The blue (red) colors indicate a decrease (increase) in temperature relative to the observed means (1958-2010).**

The case study highlights the efficiency and robustness of the downscaling steps implemented in the *pyESD* package. However, as noted in previous sections, the accuracy of the predictions generated by a GCM-ESD model coupling relies on the predictors being adequately represented by the GCMs. KS tests were performed to evaluate this for the temporal overlap (1979-2000) between the ERA5 reanalysis product and the MPI-ESM GCM output (Section 3.2.3). The KS statistic lies within the 0-1 range, with lower values indicating greater distribution similarity. For our 2-sided tests, we reject the null hypothesis (H_0 = the datasets have identical underlying distributions) for in the case of p-values being smaller than 0.05. Results from these tests show significant differences in the distribution of ERA5 and MPI-ESM when the raw monthly time series are considered, thus violating the assumptions of the PP-ESD approach. However, this issue does not persist for monthly standardized anomalies of precipitation and temperature (Fig. 11). Previous studies yielded similar results when using seasonal standardizers (Bedia et al., 2020) and principal component transformations (Benestad et al., 2015), both of which are included in the *pyESD* package.
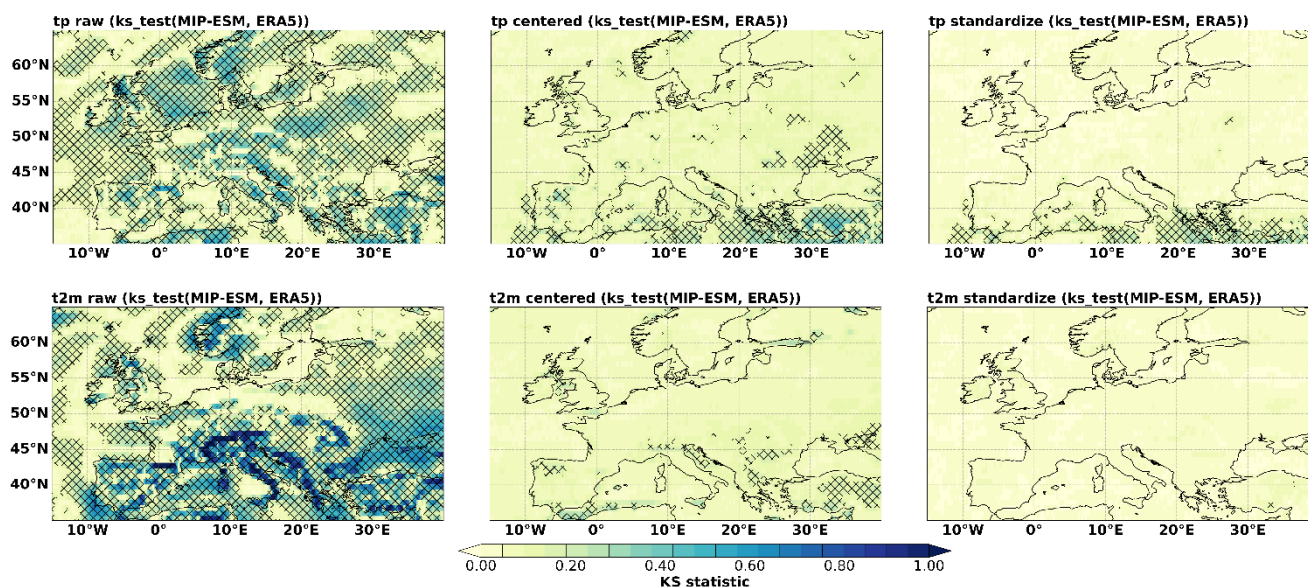
Fig. 11: KS two-sided statistical testing score maps the ERA5 reanalysis product and MPI-ESM GCM output for precipitation (top panel) and temperature (bottom panel). The KS test was applied to raw values, anomalies (centered with zero means), and standardized anomalies with unit variance values (columns from left to right, respectively). The grid boxes with black cross stipplings represent low *p* values ($p < 0.05$), suggesting statistically significant differences in distribution between the ERA5 and MPI-ESM time series.

4.5 Comparison of GCM and ESD-based predictions

A comparison of the ESD-generated annual 20a climatologies for mid-century (2040-2060) and end of the century (2080-2100) to the model output of GCMs and RCMs (i.e., EURO-CORDEX) reveal several differences. The GCMs (MPI-ESM and HadGEM2) predict ~ 20 mm/month (~ 30%) higher precipitation rates than the ESD models and RCMs. The ESD-based precipitation predictions of this study are closest to the RCM estimates, albeit ~ ≥ 5 mm/month higher in magnitude for most

of the stations (Fig. 12). The closeness of the ESD-based and RCM-based estimates underlines the added value of our ESD

780   approach for downscaling precipitation. However, there are significant (~ 4 °C) differences between the ESD-based and RCM-based temperature estimates (Fig. 13). The ESD-based temperature predictions were higher than those of the RCM, but lower than those of the GCM. Both the RCM and ESD models used boundary conditions from the same GCM (MPI-ESM). The RCM reduced the GCM temperatures by more (~ 8 °C) than the ESD models (~ 4 °C or less). This may be a reflection of both (a) the selection of GCM near-surface temperatures as predictors in the ESD models, and (b) the shrinking of regression

785   coefficients when the ESD transfer functions are determined.
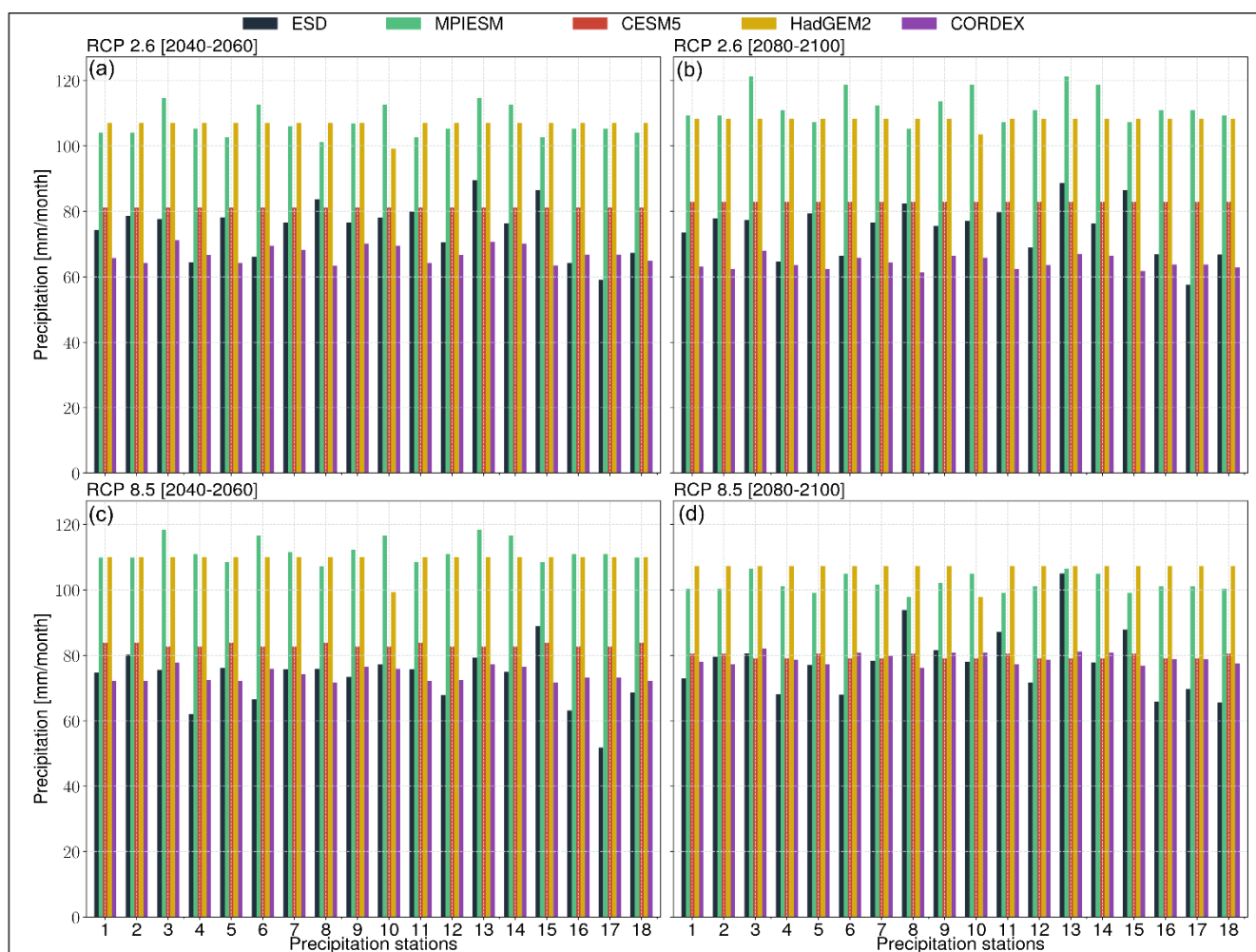
Fig. 12: Comparison of 20a annual precipitation climatologies predicted by the ESD models of this study (black), GCMs (i.e., MPI-ESM (green), CESM5 (red), HadGEM2 (gold) and RCMs (i.e., and CORDEX (purple)) for RCPs 2.6 (a, b) and 8.5 (c, d).
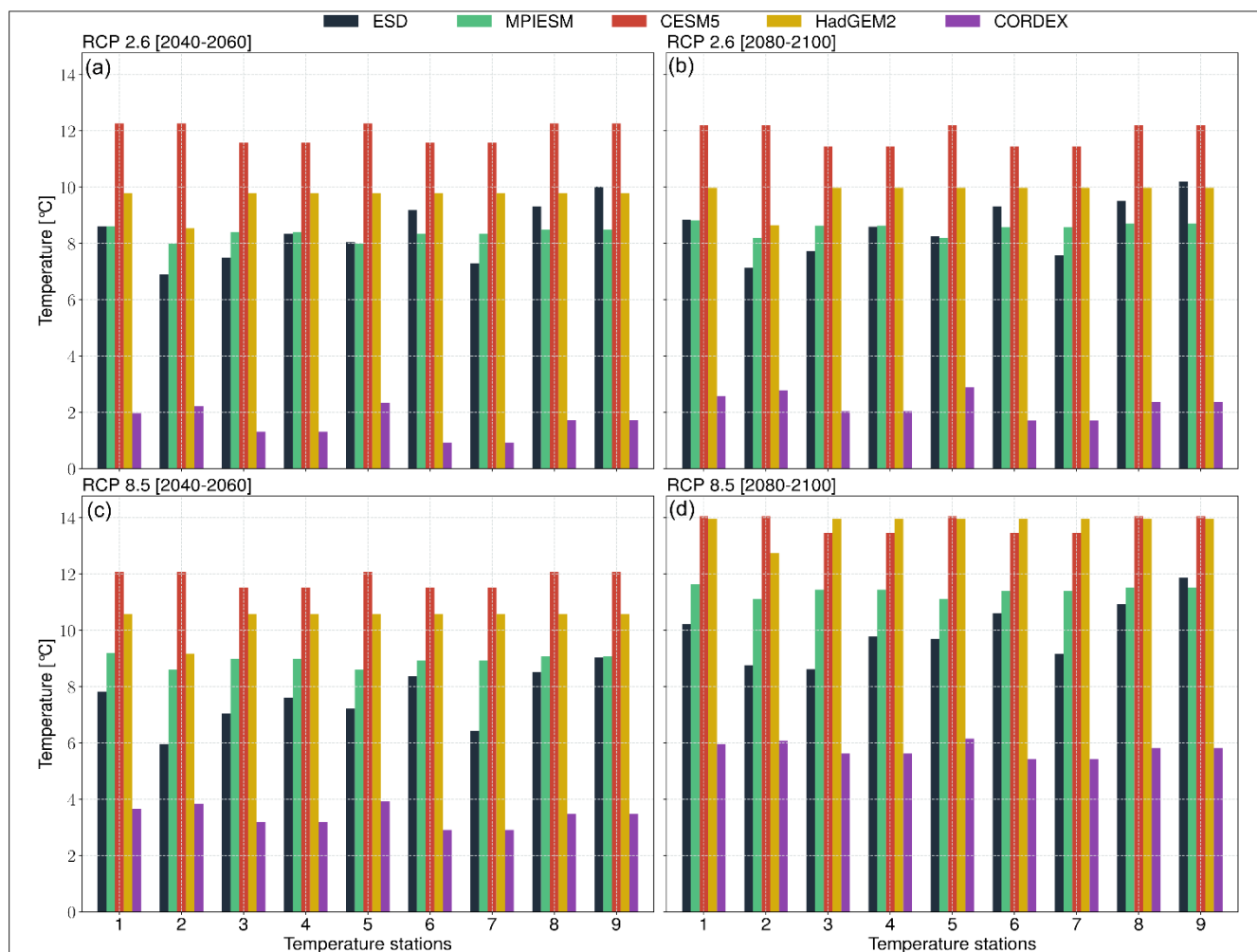
Fig. 13: Comparison of 20a annual temperature climatologies predicted by the ESD models of this study (black), GCMs (i.e., MPI-ESM (green), CESM5 (red), HadGEM2 (gold) and RCMs (i.e., and CORDEX (purple)) for RCPs 2.6 (a, b) and 8.5 (c, d).

5 Summary and Conclusion

Contemporary climate change and its impacts increase the demand for high-resolution, regional and local-scale predictions. These can be generated in a most cost-effective way through the application of the PP-ESD (perfect prognosis empirical statistical downscaling) approach. The *pyESD* python package we introduce here is a well-developed tool and modeling framework for applying, and experimenting with, PP-ESD for any climate variable (e.g., precipitation, wind speed, and temperature). The package complements existing tools through the following key specialties and strengths:

1. The package is well-structured and designed in OOP style that treats the weather stations as objects with many functionalities attributes that cover all the PP-ESD modeling routines. As a result, all modeling steps can be executed on the initialized station objects with a few lines of code.

2. The package is designed in a way that knowing its API (Application Programming Interface), which is introduced in the package's extensive documentation, is sufficient to implement all downscaling steps. In other words, no advanced knowledge of Python (or programming) is required to use the package for research purposes. On the other hand, the package's design is modular and flexible enough to allow advanced users to build on it or adjust it to their needs.

3. The package implements different predictor selection techniques (i.e., *Recursive*, *Tree-Based*, and *Sequential*) that can be manually selected and experimented with. The package allows the user to include a variety of predictors, ranging from regional near-surface temperatures to and synoptic-scale teleconnection patterns. The package features many transformation techniques such as *MonthlyStandardizer*, *PCAScalling*, etc. that can be used to reduce biases towards specific predictors.

4. The package includes a variety of machine learning techniques with different underlying principles and theorems. The package also features many ensemble models (Section 2.3), cross-validation schemes and hyperparameter optimization techniques that can easily be experimented with in a few lines of code.

5. The package's core modules are accompanied by utility functions for data pre-processing, post-processing and serialization for saving computational resources, visualization tools, and ESD-relevant statistical methods like EOF analysis, correlation and distribution similarity tests.

We demonstrated some of the package's functionalities by developing and applying ESD models to generate precipitation and temperature predictions for a sub-hydrological catchment in complex mountainous terrain in southwestern Germany. The models' performance was evaluated with different metrics and were found to perform well (e.g., $R^2 \geq 0.7$ for precipitation and $R^2 \geq 0.9$ for temperature). In order to ensure the reproducibility of the results and allow an easy practical entry for potential users, the application example uses publicly available datasets, and all the scripts used for this study are made available.

Despite the promising results of the illustrative case study, the reader is informed of the following, important limitations: Generally, the PP-ESD approach to predictions relies on the assumption that the empirical relationships between predictor and predictand remain valid through time. While statistical downscaling models have successfully been used for past climate of the pre-industrial era (Reichert et al., 1999) and Last Glacial Maximum (Vrac et al., 2007), the merit of this assumption must be evaluated on a case-by-case basis. For example, geographical boundary conditions that affect the local climate, such as topography or vegetation cover, are only implicitly considered in the empirical transfer functions. The empirical relationship between predictors and predictand may break down if these boundary conditions change significantly (e.g., Mutz and Aschauer, 2022). Furthermore, the performance of PP-ESD models also depends on the accuracy of the GCMs they are coupled to. In our case study, the developed ESD models were coupled to a single, albeit well-established, GCM (MPI-ESM). However, we generally recommend the use of GCM ensembles to prevent biases towards a specific GCM.

The current version of the package includes all functions needed to develop, evaluate and apply station-based ESD models and generate predictions of local-scale climate change. Nevertheless, the package remains under active development to expand upon its functionality. Planned improvements include an extension of functions to make *pyESD* suitable for downscaling gridded datasets or satellite observations. The grid-based analysis would contribute to the design of spatial downscaling models

835 (e.g., Chen et al., 2012; Jia et al., 2011). Moreover, we intend to expand the selection of machine learning techniques by including deep learning models that have been proven useful in downscaling (e.g., Baño-Medina et al., 2020; Quesada-Chacón et al., 2022). Finally, we intend to build a graphical, web-based interface to make the package more accessible and easy to use for researchers, students and people outside the scientific community.

840 **Appendix**

A: Supplementary results of the illustrative case study
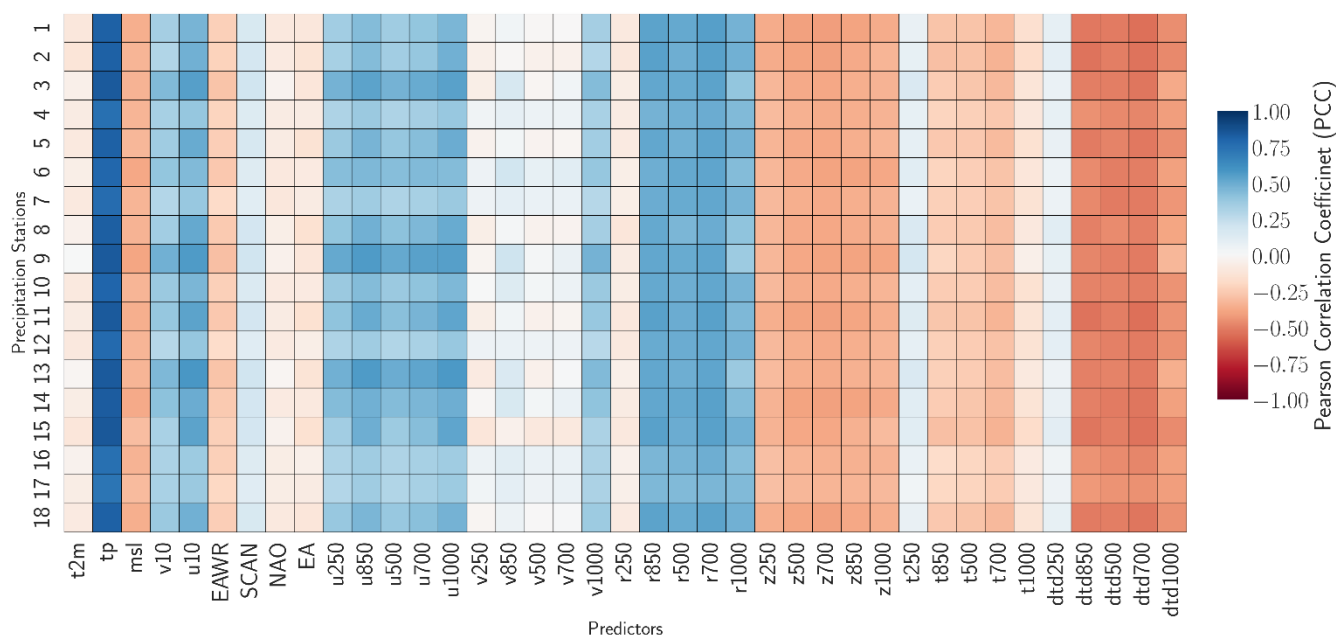
Fig. A1: Correlation between the precipitation predictand and the potential predictors listed in Table 2, expressed as PCCs.
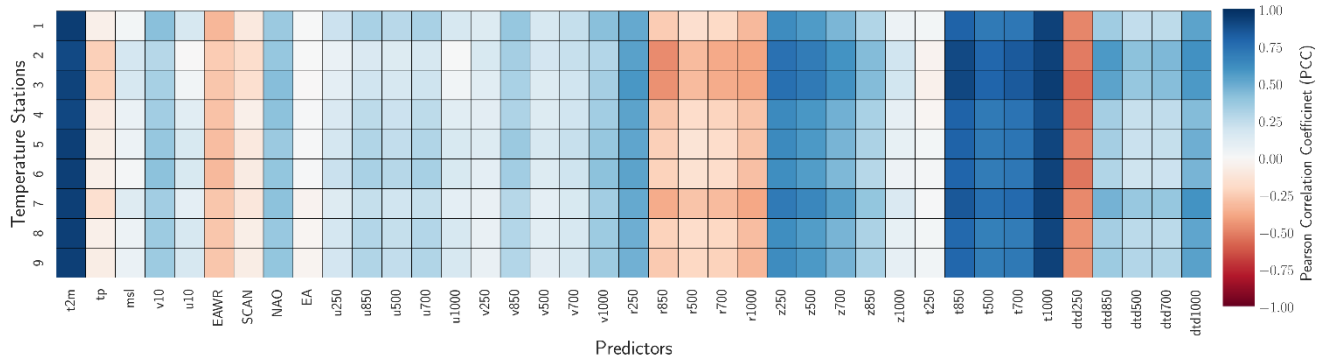
845 **Fig. A2: Correlation between the temperature predictand and the potential predictors listed in Table 2, expressed as PCCs.**
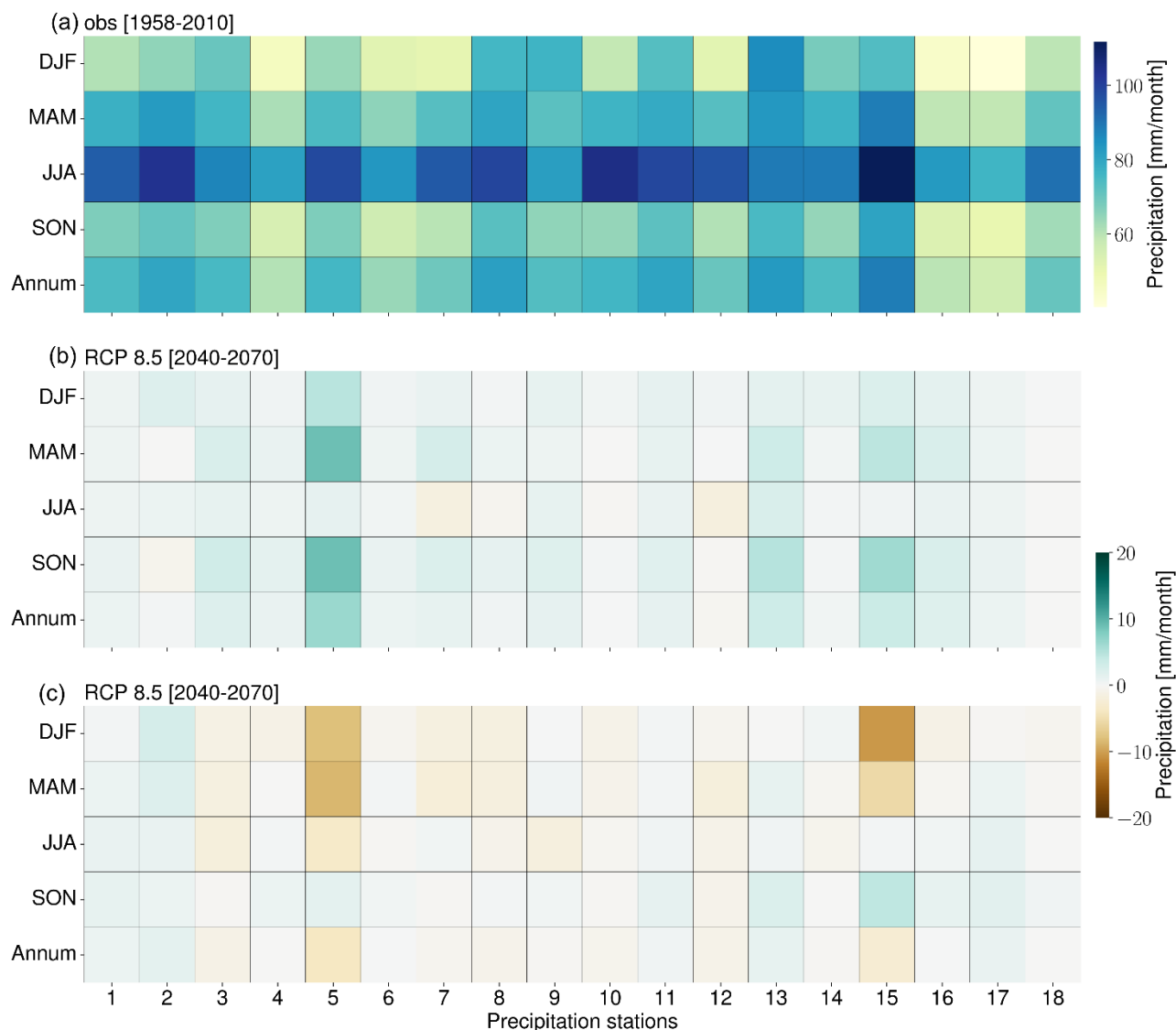
Fig. A3: Observed precipitation (1958-210), and seasonal (i.e., spring (MAM), summer (JJA), autumn (SON), and winter (DJF)) and annual mid-century (30-year) precipitation climatologies as a result of RCPs 2.6 (b), and RCP 8.5 (c) forcing. The brown (green) colors indicate a decrease (increase) in precipitation relative to the observed means (1958-2010).
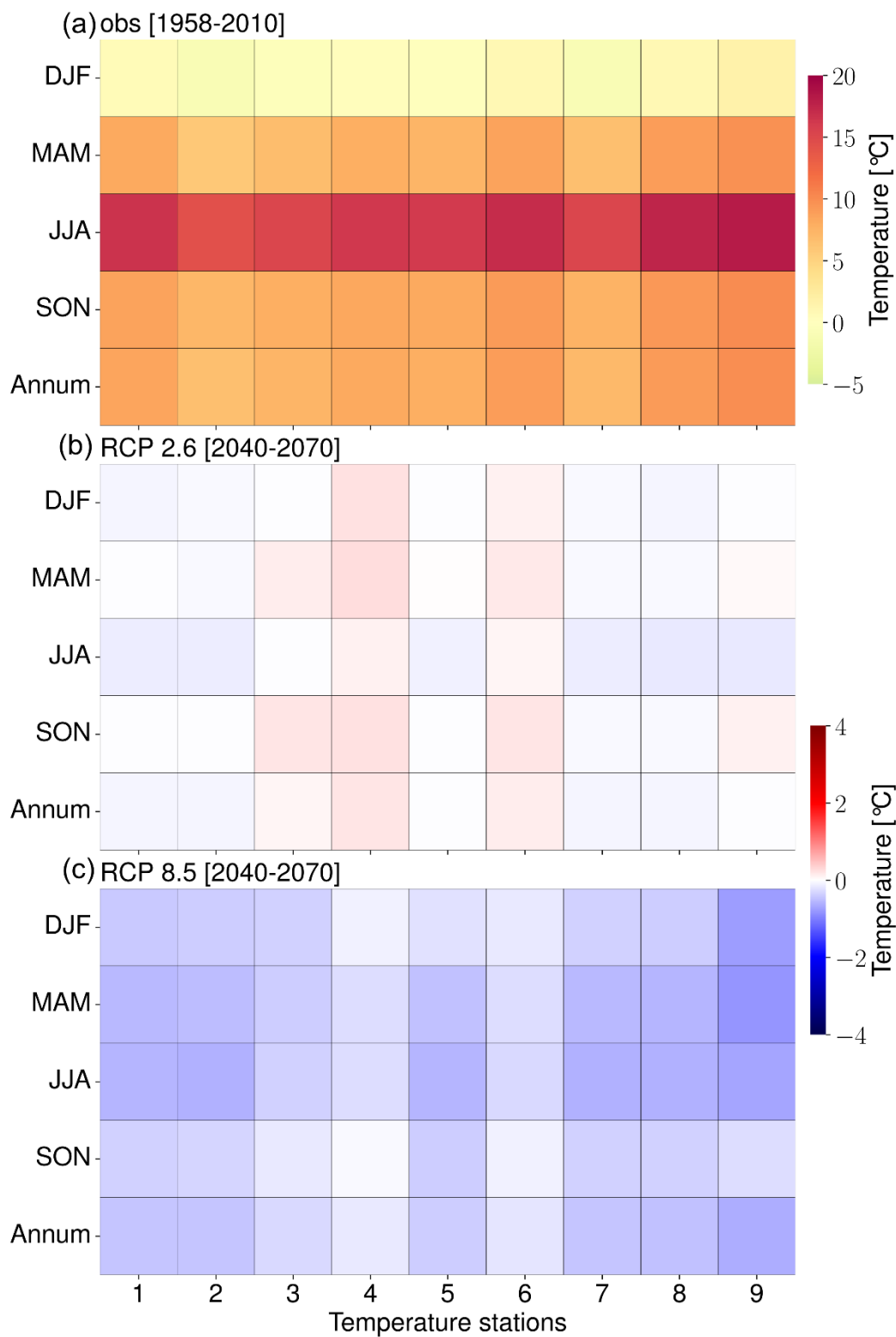
Fig. A4: Observed temperature (1958-210), and seasonal (i.e., spring (MAM), summer (JJA), autumn (SON), and winter (DJF)) and annual mid-century (30-year) temperature climatologies as a result of RCPs 2.6 (b), and RCP 8.5 (c) forcing. The blue (red) colors indicate a decrease (increase) in temperature relative to the observed means (1958-2010).
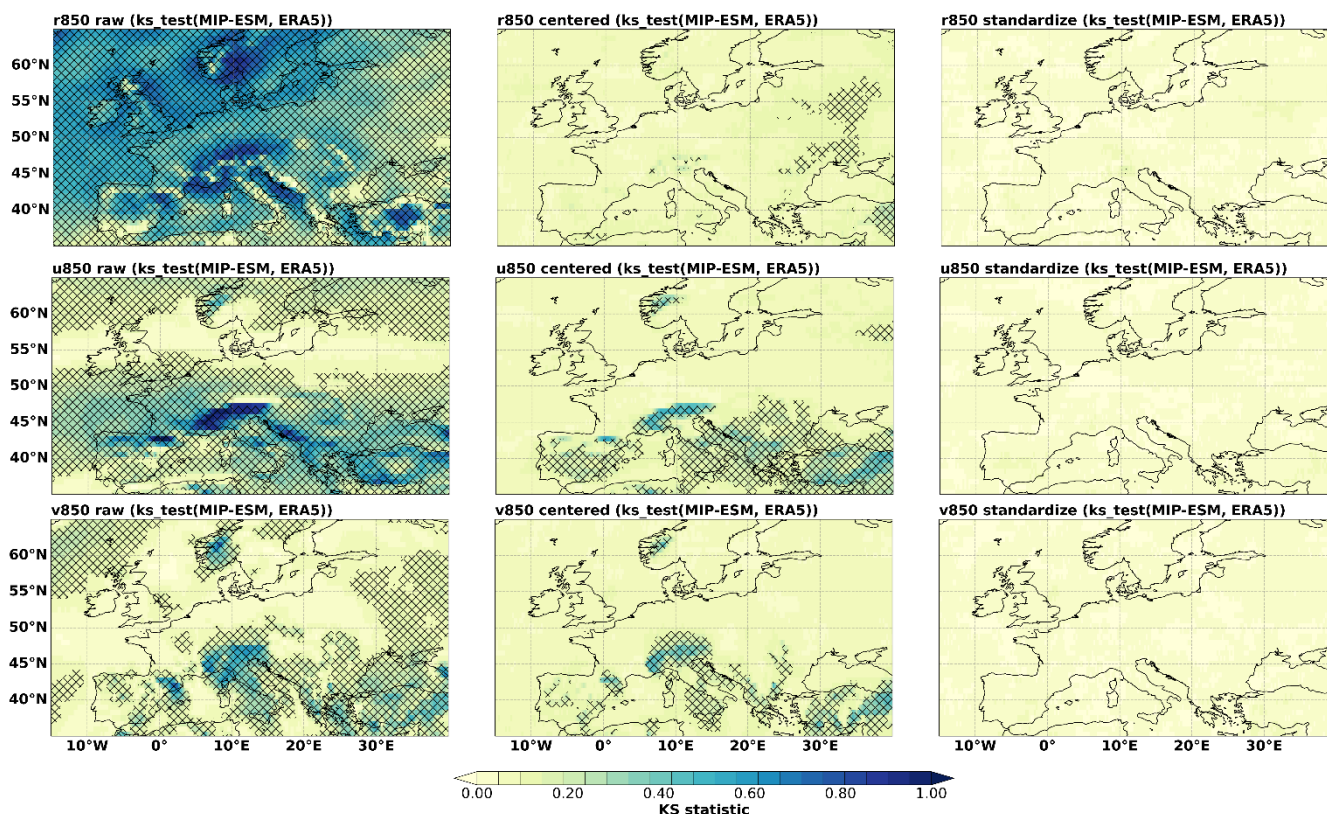
855 **Fig. A5: KS two-sided statistical testing score maps the ERA5 reanalysis product and MPI-ESM GCM output for relative humidity (top panel), zonal winds velocity (middle panel), and meridional winds velocity (bottom panel) on 850 hPa. The KS test was applied to raw values, anomalies (centered with zero means), and standardized anomalies with unit variance values (columns from left to right, respectively). The grid boxes with black cross stipplings represent low p values (p < 0.05), suggesting statistically significant differences in distribution between the ERA5 and MPI-ESM time series.**

860 **Data Availability**

The study's illustrative case study relies on publicly available datasets. More specifically, the precipitation and temperature datasets are accessible through the Climate Data Centre of the DWD (https://cdc.dwd.de/portal/). The sub-catchment datasets used in this study are interactively available through https://cdc.dwd.de/portal/202209231028/mapview and https://cdc.dwd.de/portal/202209231028/mapview for precipitation and temperature stations, respectively. The ERA5

865 reanalysis datasets can also be downloaded through Copernicus Climate Data Store (CDS) (https://doi.org/10.24381/cds.6860a573 for pressure level and https://doi.org/10.24381/cds.68d2bb30 for surface level variables). However, the processed weather stations and the serialized pickle files of the regional means of the predictors for all the stations are provided as part of the supporting material (https://doi.org/10.5281/zenodo.7767681). The MPI-ESM GCM

datasets used as simulated predictors can also be downloaded from the CDS by selecting the MPI-ESM-LR as the model for
870   the AMIP, RCP 2.6, 4.5 and 8.5 experiments: https://doi.org/10.24381/cds.3b4b5bc9 pressure levels variables and
https://doi.org/10.24381/cds.9d44a987 for surface variables. Moreover, the station-based downscaling estimates of future
climate scenarios for all the stations are also included in the supporting material (https://doi.org/10.5281/zenodo.7767681).

Code Availability

The pyESD (version 1.0.1) software including the documentation website source files is available through many platforms:
875   - Github: https://github.com/Dan-Boat/PyESD
- Python package index (PyPI): https://pypi.org/project/PyESD/
- Zenodo (v1.0.1 release): https://doi.org/10.5281/zenodo.7767629

880   Developer: Daniel Boateng, University of Tübingen

Hardware requirements: general-purpose computer

Programming language: Python (Version 3.7 or later)

The installation of the package and its required dependencies are highlighted in the documentation website: https://dan-boat.github.io/PyESD/. The usage of the package and its functionalities are also presented in the documentation. The control
885   scripts of the study's illustrative case study are also provided as part of the supporting material
(https://doi.org/10.5281/zenodo.7767681) and also presented in the example section of the documentation.

Acknowledgment

This study was partially supported by the German Science Foundation (DFG) grants MU4188/3-1 and MU4188/1-1, awarded
to Sebastian G. Mutz. We acknowledge the World Climate Research Programme, which, through its Working Group on
890   Coupled Modelling, coordinated and promoted CMIP5. We thank the climate modeling groups for producing and making
available their model output, the Earth System Grid Federation (ESGF) for archiving the data and providing access, and the
multiple funding agencies who support CMIP5 and ESGF. We also thank the European Centre for Medium Range Weather
Forecasts for providing the ERA5 data product, and the Deutsche Wetterdienst (DWD) for providing the weather station
records. Finally, we acknowledge support from the Open Access Publishing Fund of the University of Tübingen (enabled and
895   organized by Projekt DEAL).

Author contribution

D.B: pyESD software development, conceptualization, modeling, data analysis, visualization, and writing of the original manuscript. S.G.M.: Supervision, manuscript editing, and funding acquisition.

Competing interests

900 The authors declare that they have no conflict of interest.

References

Anandhi, A., Srinivas, V. V., Nanjundiah, R. S., and Nagesh Kumar, D.: Downscaling precipitation to river basin in India for IPCC SRES scenarios using support vector machine, International Journal of Climatology, 28, 401–420,
905 https://doi.org/10.1002/joc.1529, 2008.

Arlot, S. and Celisse, A.: A survey of cross-validation procedures for model selection, Statistics Surveys, 4, 40–79, https://doi.org/10.1214/09-SS054, 2010.

Balasundaram, S. and Tanveer, M.: On Lagrangian twin support vector regression, Neural Computing and Applications, 22, 257–267, 2013.

910 Baño-Medina, J., Manzanas, R., and Gutiérrez, J. M.: Configuration and intercomparison of deep learning neural models for statistical downscaling, Geoscientific Model Development, 13, 2109–2124, https://doi.org/10.5194/gmd-13-2109-2020, 2020.

Bárdossy, A.: Atmospheric circulation pattern classification for South-West Germany using hydrological variables, Physics and Chemistry of the Earth, Parts A/B/C, 35, 498–506, https://doi.org/10.1016/j.pce.2010.02.007, 2010.

Barnston, A. G. and Livezey, R. E.: Classification, Seasonality and Persistence of Low-Frequency Atmospheric Circulation
915 Patterns, Monthly Weather Review, 115, 1083–1126, https://doi.org/10.1175/1520-0493(1987)115<1083:CSAPOL>2.0.CO;2, 1987.

Bedia, J., Baño-Medina, J., Legasa, M. N., Iturbide, M., Manzanas, R., Herrera, S., Casanueva, A., San-Martín, D., Cofiño, A. S., and Gutiérrez, J. M.: Statistical downscaling with the downscaleR package (v3.1.0): contribution to the VALUE intercomparison experiment, Geoscientific Model Development, 13, 1711–1735,
920 https://doi.org/10.5194/gmd-13-1711-2020, 2020.

Bell, B., Hersbach, H., Simmons, A., Berrisford, P., Dahlgren, P., Horányi, A., Muñoz-Sabater, J., Nicolas, J., Radu, R., Schepers, D., Soci, C., Villaume, S., Bidlot, J.-R., Haimberger, L., Woollen, J., Buontempo, C., and Thépaut, J.-N.: The ERA5 global reanalysis: Preliminary extension to 1950, Quarterly Journal of the Royal Meteorological Society, 147, 4186–4227, https://doi.org/10.1002/qj.4174, 2021.

925 Benestad, R. E., Mezghani, A., and M. Parding, K.: `esd' - The Empirical-Statistical Downscaling tool \& its visualisation capabilities., https://doi.org/10.6084/m9.figshare.1454425.v1, 2015a.

Benestad, R. E., Chen, D., Mezghani, A., Fan, L., and Parding, K.: On using principal components to represent stations in empirical–statistical downscaling, Tellus A: Dynamic Meteorology and Oceanography, 67, 28326, https://doi.org/10.3402/tellusa.v67.28326, 2015b.

930 Bergmeir, C. and Benítez, J. M.: On the use of cross-validation for time series predictor evaluation, Information Sciences, 191, 192–213, https://doi.org/10.1016/j.ins.2011.12.028, 2012.

Bergstra, J. and Bengio, Y.: Random search for hyper-parameter optimization., Journal of machine learning research, 13, 2012.

Bergstra, J., Bardenet, R., Bengio, Y., and Kégl, B.: Algorithms for Hyper-Parameter Optimization, in: Advances in Neural Information Processing Systems, 2011.

935 Bishop, C. M. and Nasrabadi, N. M.: Pattern recognition and machine learning, Springer, 2006.

Boateng, D., Mutz, S. G., Ballian, A., Meijers, M. J. M., Methner, K., Botsyun, S., Mulch, A., and Ehlers, T. A.: The effects of diachronous surface uplift of the European Alps on regional climate and the oxygen isotopic composition of precipitation, Earth System Dynamics Discussions, 1–45, https://doi.org/10.5194/esd-2022-48, 2022.

Boé, J., Terray, L., Martin, E., and Habets, F.: Projected changes in components of the hydrological cycle in French river
940 basins during the 21st century, Water Resources Research, 45, https://doi.org/10.1029/2008WR007437, 2009.

Bottou, L.: Stochastic gradient learning in neural networks, Proceedings of Neuro-Nımes, 91, 12, 1991.

Brands, S., Gutiérrez, J. M., Herrera, S., and Cofiño, A. S.: On the Use of Reanalysis Data for Downscaling, Journal of Climate, 25, 2517–2526, https://doi.org/10.1175/JCLI-D-11-00251.1, 2012.

Breiman, L.: Bagging predictors, Machine learning, 24, 123–140, 1996a.

945 Breiman, L.: Stacked regressions, Mach Learn, 24, 49–64, https://doi.org/10.1007/BF00117832, 1996b.

Breiman, L.: Random forests, Machine learning, 45, 5–32, 2001.

Chandler, R. E. and Wheater, H. S.: Analysis of rainfall variability using generalized linear models: A case study from the west of Ireland, Water Resources Research, 38, 10-1-10–11, https://doi.org/10.1029/2001WR000906, 2002.

Chen, J., Brissette, F. P., and Leconte, R.: Coupling statistical and dynamical methods for spatial downscaling of precipitation,
950 Climatic Change, 114, 509–526, https://doi.org/10.1007/s10584-012-0452-2, 2012.

Chen, S.-T., Yu, P.-S., and Tang, Y.-H.: Statistical downscaling of daily precipitation using support vector machines and multivariate analysis, Journal of Hydrology, 385, 13–22, https://doi.org/10.1016/j.jhydrol.2010.01.021, 2010.

Chen, T. and Guestrin, C.: XGBoost: A Scalable Tree Boosting System, in: Proceedings of the 22nd ACM SIGKDD International Conference on Knowledge Discovery and Data Mining, KDD '16: The 22nd ACM SIGKDD International
955 Conference on Knowledge Discovery and Data Mining, San Francisco California USA, 785–794, https://doi.org/10.1145/2939672.2939785, 2016.

Chen, X. and Jeong, J. C.: Enhanced recursive feature elimination, in: Sixth International Conference on Machine Learning and Applications (ICMLA 2007), Sixth International Conference on Machine Learning and Applications (ICMLA 2007), 429–435, https://doi.org/10.1109/ICMLA.2007.35, 2007.

960 Colette, A., Granier, C., Hodnebrog, Ø., Jakobs, H., Maurizi, A., Nyiri, A., Rao, S., Amann, M., Bessagnet, B., D'Angiola, A., Gauss, M., Heyes, C., Klimont, Z., Meleux, F., Memmesheimer, M., Mieville, A., Rouïl, L., Russo, F., Schucht, S., Simpson, D., Stordal, F., Tampieri, F., and Vrac, M.: Future air quality in Europe: a multi-model assessment of projected exposure to ozone, Atmospheric Chemistry and Physics, 12, 10613–10630, https://doi.org/10.5194/acp-12-10613-2012, 2012.

Colle, B. A.: Sensitivity of Orographic Precipitation to Changing Ambient Conditions and Terrain Geometries: An Idealized
965 Modeling Perspective, J. Atmos. Sci., 61, 588–606, https://doi.org/10.1175/1520-0469(2004)061<0588:SOOPTC>2.0.CO;2, 2004.

Collins, W. J., Bellouin, N., Doutriaux-Boucher, M., Gedney, N., Hinton, T., Jones, C. D., Liddicoat, S., Martin, G., O'Connor, F., and Rae, J.: Evaluation of the HadGEM2 model, Met Office Exeter, UK, 2008.

Cristianini, N. and Shawe-Taylor, J.: An introduction to support vector machines and other kernel-based learning methods,
970 Cambridge university press, 2000.

Das, D., Dy, J., Ross, J., Obradovic, Z., and Ganguly, A. R.: Non-parametric Bayesian mixture of sparse regressions with application towards feature selection for statistical downscaling, Nonlinear Processes in Geophysics, 21, 1145–1157, https://doi.org/10.5194/npg-21-1145-2014, 2014.

Dau, Q. V., Kuntiyawichai, K., and Adeloye, A. J.: Future Changes in Water Availability Due to Climate Change Projections
975 for Huong Basin, Vietnam, Environ. Process., 8, 77–98, https://doi.org/10.1007/s40710-020-00475-y, 2021.

Diaz, G. I., Fokoue-Nkoutche, A., Nannicini, G., and Samulowitz, H.: An effective algorithm for hyperparameter optimization of neural networks, IBM Journal of Research and Development, 61, 9–1, 2017.

Dietterich, T. G.: Ensemble Methods in Machine Learning, in: Multiple Classifier Systems, Berlin, Heidelberg, 1–15, https://doi.org/10.1007/3-540-45014-9_1, 2000.

980 Efron, B., Hastie, T., Johnstone, I., and Tibshirani, R.: Least angle regression, The Annals of Statistics, 32, 407–499, https://doi.org/10.1214/009053604000000067, 2004.

Errico, R. M., Stensrud, D. J., and Raeder, K. D.: Estimation of the error distributions of precipitation produced by convective parametrization schemes, Quarterly Journal of the Royal Meteorological Society, 127, 2495–2512, 2001.

Fan, J., Wu, L., Zheng, J., and Zhang, F.: Medium-range forecasting of daily reference evapotranspiration across China using
985 numerical weather prediction outputs downscaled by extreme gradient boosting, Journal of Hydrology, 601, 126664, https://doi.org/10.1016/j.jhydrol.2021.126664, 2021.

Fealy, R. and Sweeney, J.: Statistical downscaling of precipitation for a selection of sites in Ireland employing a generalised linear modelling approach, International Journal of Climatology, 27, 2083–2094, https://doi.org/10.1002/joc.1506, 2007.

Feldmann, H., Schädler, G., Panitz, H.-J., and Kottmeier, C.: Near future changes of extreme precipitation over complex terrain
990 in Central Europe derived from high resolution RCM ensemble simulations, International Journal of Climatology, 33, 1964–1977, https://doi.org/10.1002/joc.3564, 2013.

Ferri, F. J., Pudil, P., Hatef, M., and Kittler, J.: Comparative study of techniques for large-scale feature selection* *This work was supported by a SERC grant GR/E 97549. The first author was also supported by a FPI grant from the Spanish MEC, PF92

73546684, in: Machine Intelligence and Pattern Recognition, vol. 16, edited by: Gelsema, E. S. and Kanal, L. S., North-Holland, 403–413, https://doi.org/10.1016/B978-0-444-81892-8.50040-7, 1994.

Field, C. B. and Barros, V. R.: Climate Change 2014 – Impacts, Adaptation and Vulnerability: Regional Aspects, Cambridge University Press, 695 pp., 2014.

Freund, Y. and Schapire, R. E.: A Decision-Theoretic Generalization of On-Line Learning and an Application to Boosting, Journal of Computer and System Sciences, 55, 119–139, https://doi.org/10.1006/jcss.1997.1504, 1997.

Friedman, J. H.: Greedy function approximation: a gradient boosting machine, Annals of statistics, 1189–1232, 2001.

Friedman, J. H.: Stochastic gradient boosting, Computational Statistics & Data Analysis, 38, 367–378, https://doi.org/10.1016/S0167-9473(01)00065-2, 2002.

Gardner, M. W. and Dorling, S. R.: Artificial neural networks (the multilayer perceptron)—a review of applications in the atmospheric sciences, Atmospheric environment, 32, 2627–2636, 1998.

Gareth, J., Daniela, W., Trevor, H., and Robert, T.: An introduction to statistical learning: with applications in R, Spinger, 2013.

Geurts, P., Ernst, D., and Wehenkel, L.: Extremely randomized trees, Machine learning, 63, 3–42, 2006.

Ghosh, S. and Mujumdar, P. P.: Statistical downscaling of GCM simulations to streamflow using relevance vector machine, Advances in Water Resources, 31, 132–146, https://doi.org/10.1016/j.advwatres.2007.07.005, 2008.

Giorgi, F. and Mearns, L. O.: Approaches to the simulation of regional climate change: A review, Reviews of Geophysics, 29, 191–216, https://doi.org/10.1029/90RG02636, 1991.

Gobiet, A., Kotlarski, S., Beniston, M., Heinrich, G., Rajczak, J., and Stoffel, M.: 21st century climate change in the European Alps—A review, Science of The Total Environment, 493, 1138–1151, https://doi.org/10.1016/j.scitotenv.2013.07.050, 2014.

Gu, J., Liu, S., Zhou, Z., Chalov, S. R., and Zhuang, Q.: A Stacking Ensemble Learning Model for Monthly Rainfall Prediction in the Taihu Basin, China, Water, 14, 492, https://doi.org/10.3390/w14030492, 2022.

Gutiérrez, J. M., San-Martín, D., Cofiño, A. S., Herrera, S., Manzanas, R., and Frías, M. D.: User guide of the ENSEMBLES downscaling portal (version 2), 2011.

Gutiérrez, J. M., San-Martín, D., Brands, S., Manzanas, R., and Herrera, S.: Reassessing Statistical Downscaling Techniques for Their Robust Application under Climate Change Conditions, Journal of Climate, 26, 171–188, https://doi.org/10.1175/JCLI-D-11-00687.1, 2013.

Gutiérrez, J. M., Maraun, D., Widmann, M., Huth, R., Hertig, E., Benestad, R., Roessler, O., Wibig, J., Wilcke, R., Kotlarski, S., San Martín, D., Herrera, S., Bedia, J., Casanueva, A., Manzanas, R., Iturbide, M., Vrac, M., Dubrovsky, M., Ribalaygua, J., Pórtoles, J., Räty, O., Räisänen, J., Hingray, B., Raynaud, D., Casado, M. J., Ramos, P., Zerenner, T., Turco, M., Bosshard, T., Štěpánek, P., Bartholy, J., Pongracz, R., Keller, D. E., Fischer, A. M., Cardoso, R. M., Soares, P. M. M., Czernecki, B., and Pagé, C.: An intercomparison of a large ensemble of statistical downscaling methods over Europe: Results from the VALUE perfect predictor cross-validation experiment, International Journal of Climatology, 39, 3750–3785, https://doi.org/10.1002/joc.5462, 2019.

Hammami, D., Lee, T. S., Ouarda, T. B. M. J., and Lee, J.: Predictor selection for downscaling GCM data with LASSO, Journal of Geophysical Research: Atmospheres, 117, https://doi.org/10.1029/2012JD017864, 2012.

1030 Hanel, M., Kožín, R., Heřmanovský, M., and Roub, R.: An R package for assessment of statistical downscaling methods for hydrological climate change impact studies, Environmental Modelling & Software, 95, 22–28, https://doi.org/10.1016/j.envsoft.2017.03.036, 2017.

Hastie, T., Friedman, J., and Tibshirani, R.: The Elements of Statistical Learning, Springer New York, New York, NY, https://doi.org/10.1007/978-0-387-21606-5, 2001.

1035 He, X., Chaney, N. W., Schleiss, M., and Sheffield, J.: Spatial downscaling of precipitation using adaptable random forests, Water Resources Research, 52, 8217–8237, https://doi.org/10.1002/2016WR019034, 2016.

Hecht-Nielsen, R.: Theory of the backpropagation neural network, in: Neural networks for perception, Elsevier, 65–93, 1992.

Hersbach, H., Bell, B., Berrisford, P., Hirahara, S., Horányi, A., Muñoz-Sabater, J., Nicolas, J., Peubey, C., Radu, R., Schepers, D., Simmons, A., Soci, C., Abdalla, S., Abellan, X., Balsamo, G., Bechtold, P., Biavati, G., Bidlot, J., Bonavita, M., De Chiara,

1040 G., Dahlgren, P., Dee, D., Diamantakis, M., Dragani, R., Flemming, J., Forbes, R., Fuentes, M., Geer, A., Haimberger, L., Healy, S., Hogan, R. J., Hólm, E., Janisková, M., Keeley, S., Laloyaux, P., Lopez, P., Lupu, C., Radnoti, G., de Rosnay, P., Rozum, I., Vamborg, F., Villaume, S., and Thépaut, J.-N.: The ERA5 global reanalysis, Quarterly Journal of the Royal Meteorological Society, 146, 1999–2049, https://doi.org/10.1002/qj.3803, 2020.

Hertig, E., Maraun, D., Bartholy, J., Pongracz, R., Vrac, M., Mares, I., Gutiérrez, J. M., Wibig, J., Casanueva, A., and Soares,

1045 P. M. M.: Comparison of statistical downscaling methods with respect to extreme events over Europe: Validation results from the perfect predictor experiment of the COST Action VALUE, International Journal of Climatology, 39, 3846–3867, https://doi.org/10.1002/joc.5469, 2019.

Hewitson, B. C., Daron, J., Crane, R. G., Zermoglio, M. F., and Jack, C.: Interrogating empirical-statistical downscaling, Climatic Change, 122, 539–554, https://doi.org/10.1007/s10584-013-1021-z, 2014.

1050 Hodgkins, G. A., Whitfield, P. H., Burn, D. H., Hannaford, J., Renard, B., Stahl, K., Fleig, A. K., Madsen, H., Mediero, L., Korhonen, J., Murphy, C., and Wilson, D.: Climate-driven variability in the occurrence of major floods across North America and Europe, Journal of Hydrology, 552, 704–717, https://doi.org/10.1016/j.jhydrol.2017.07.027, 2017.

Hofmann, T., Schölkopf, B., and Smola, A. J.: Kernel methods in machine learning, The Annals of Statistics, 36, 1171–1220, https://doi.org/10.1214/009053607000000677, 2008.

1055 Hoyer, S. and Hamman, J.: xarray: N-D labeled Arrays and Datasets in Python, Journal of Open Research Software, 5, 10, https://doi.org/10.5334/jors.148, 2017.

Hurrell, J. W.: Decadal Trends in the North Atlantic Oscillation: Regional Temperatures and Precipitation, Science, 269, 676–679, https://doi.org/10.1126/science.269.5224.676, 1995.

Hurrell, J. W. and Van Loon, H.: Decadal Variations in Climate Associated with the North Atlantic Oscillation, in: Climatic

1060 Change at High Elevation Sites, edited by: Diaz, H. F., Beniston, M., and Bradley, R. S., Springer Netherlands, Dordrecht, 69–94, https://doi.org/10.1007/978-94-015-8905-5_4, 1997.

Huth, R.: Statistical downscaling in central Europe: evaluation of methods and potential predictors, Clim. Res., 13, 91–101, https://doi.org/10.3354/cr013091, 1999.

Huth, R.: Sensitivity of Local Daily Temperature Change Estimates to the Selection of Downscaling Models and Predictors, Journal of Climate, 17, 640–652, https://doi.org/10.1175/1520-0442(2004)017<0640:SOLDTC>2.0.CO;2, 2004.

Iturbide, M., Bedia, J., Herrera, S., Baño-Medina, J., Fernández, J., Frías, M. D., Manzanas, R., San-Martín, D., Cimadevilla, E., Cofiño, A. S., and Gutiérrez, J. M.: The R-based climate4R open framework for reproducible climate data access and post-processing, Environmental Modelling & Software, 111, 42–54, https://doi.org/10.1016/j.envsoft.2018.09.009, 2019.

Jakob Themeßl, M., Gobiet, A., and Leuprecht, A.: Empirical-statistical downscaling and error correction of daily precipitation from regional climate models, International Journal of Climatology, 31, 1530–1544, https://doi.org/10.1002/joc.2168, 2011.

Jia, S., Zhu, W., Lǚ, A., and Yan, T.: A statistical spatial downscaling algorithm of TRMM precipitation based on NDVI and DEM in the Qaidam Basin of China, Remote Sensing of Environment, 115, 3069–3079, https://doi.org/10.1016/j.rse.2011.06.009, 2011.

Jordan, M. I. and Mitchell, T. M.: Machine learning: Trends, perspectives, and prospects, Science, 349, 255–260, https://doi.org/10.1126/science.aaa8415, 2015.

Kageyama, M., Braconnot, P., Harrison, S. P., Haywood, A. M., Jungclaus, J. H., Otto-Bliesner, B. L., Peterschmitt, J.-Y., Abe-Ouchi, A., Albani, S., Bartlein, P. J., Brierley, C., Crucifix, M., Dolan, A., Fernandez-Donado, L., Fischer, H., Hopcroft, P. O., Ivanovic, R. F., Lambert, F., Lunt, D. J., Mahowald, N. M., Peltier, W. R., Phipps, S. J., Roche, D. M., Schmidt, G. A., Tarasov, L., Valdes, P. J., Zhang, Q., and Zhou, T.: The PMIP4 contribution to CMIP6 – Part 1: Overview and over-arching analysis plan, Geosci. Model Dev., 11, 1033–1057, https://doi.org/10.5194/gmd-11-1033-2018, 2018.

Kay, J. E., Deser, C., Phillips, A., Mai, A., Hannay, C., Strand, G., Arblaster, J. M., Bates, S. C., Danabasoglu, G., Edwards, J., Holland, M., Kushner, P., Lamarque, J.-F., Lawrence, D., Lindsay, K., Middleton, A., Munoz, E., Neale, R., Oleson, K., Polvani, L., and Vertenstein, M.: The Community Earth System Model (CESM) Large Ensemble Project: A Community Resource for Studying Climate Change in the Presence of Internal Climate Variability, Bulletin of the American Meteorological Society, 96, 1333–1349, https://doi.org/10.1175/BAMS-D-13-00255.1, 2015.

Kingma, D. P. and Ba, J.: Adam: A method for stochastic optimization, arXiv preprint arXiv:1412.6980, 2014.

Kumar, V. and Minz, S.: Feature selection: a literature review, SmartCR, 4, 211–229, 2014.

Kunstmann, H., Schneider, K., Forkel, R., and Knoche, R.: Impact analysis of climate change for an Alpine catchment using high resolution dynamic downscaling of ECHAM4 time slices, Hydrology and Earth System Sciences, 8, 1031–1045, https://doi.org/10.5194/hess-8-1031-2004, 2004.

Lachenbruch, P. A. and Mickey, M. R.: Estimation of Error Rates in Discriminant Analysis, Technometrics, 10, 1–11, https://doi.org/10.1080/00401706.1968.10490530, 1968.

Laflamme, E. M., Linder, E., and Pan, Y.: Statistical downscaling of regional climate model output to achieve projections of precipitation extremes, Weather and Climate Extremes, 12, 15–23, https://doi.org/10.1016/j.wace.2015.12.001, 2016.

1095   Lau, W. K.-M., Wu, H.-T., and Kim, K.-M.: A canonical response of precipitation characteristics to global warming from CMIP5 models, Geophysical Research Letters, 40, 3163–3169, https://doi.org/10.1002/grl.50420, 2013.

Leblanc, M. and Tibshirani, R.: Combining Estimates in Regression and Classification, Journal of the American Statistical Association, 91, 1641–1650, https://doi.org/10.1080/01621459.1996.10476733, 1996.

Li, J., Pollinger, F., and Paeth, H.: Comparing the Lasso Predictor-Selection and Regression Method with Classical Approaches

1100   of Precipitation Bias Adjustment in Decadal Climate Predictions, Monthly Weather Review, 148, 4339–4351, https://doi.org/10.1175/MWR-D-19-0302.1, 2020.

Liu, J., Yuan, D., Zhang, L., Zou, X., and Song, X.: Comparison of Three Statistical Downscaling Methods and Ensemble Downscaling Method Based on Bayesian Model Averaging in Upper Hanjiang River Basin, China, Advances in Meteorology, 2016, e7463963, https://doi.org/10.1155/2016/7463963, 2015.

1105   Lorenz, E. N.: Atmospheric Predictability as Revealed by Naturally Occurring Analogues, Journal of the Atmospheric Sciences, 26, 636–646, https://doi.org/10.1175/1520-0469(1969)26<636:APARBN>2.0.CO;2, 1969.

Ludwig, R., Taschner, S., and Mauser, W.: Modelling floods in the Ammer catchment: limitations and challenges with a coupled meteo-hydrological model approach, Hydrology and Earth System Sciences, 7, 833–847, https://doi.org/10.5194/hess-7-833-2003, 2003.

1110   MacKay, D. J.: Bayesian interpolation, Neural computation, 4, 415–447, 1992.

Maraun, D. and Widmann, M. (Eds.): Structure of Statistical Downscaling Methods, in: Statistical Downscaling and Bias Correction for Climate Research, Cambridge University Press, Cambridge, 135–140, https://doi.org/10.1017/9781107588783.011, 2018.

Maraun, D., Wetterhall, F., Ireson, A. M., Chandler, R. E., Kendon, E. J., Widmann, M., Brienen, S., Rust, H. W., Sauter, T.,

1115   Themeßl, M., Venema, V. K. C., Chun, K. P., Goodess, C. M., Jones, R. G., Onof, C., Vrac, M., and Thiele-Eich, I.: Precipitation downscaling under climate change: Recent developments to bridge the gap between dynamical models and the end user, Reviews of Geophysics, 48, https://doi.org/10.1029/2009RG000314, 2010.

Maraun, D., Widmann, M., and Gutiérrez, J. M.: Statistical downscaling skill under present climate conditions: A synthesis of the VALUE perfect predictor experiment, International Journal of Climatology, 39, 3692–3703,

1120   https://doi.org/10.1002/joc.5877, 2019a.

Maraun, D., Huth, R., Gutiérrez, J. M., Martín, D. S., Dubrovsky, M., Fischer, A., Hertig, E., Soares, P. M. M., Bartholy, J., Pongrácz, R., Widmann, M., Casado, M. J., Ramos, P., and Bedia, J.: The VALUE perfect predictor experiment: Evaluation of temporal variability, International Journal of Climatology, 39, 3786–3818, https://doi.org/10.1002/joc.5222, 2019b.

Markatou, M., Tian, H., Biswas, S., and Hripcsak, G. M.: Analysis of variance of cross-validation estimators of the

1125   generalization error, 2005.

Marzban, C., Sandgathe, S., and Kalnay, E.: MOS, Perfect Prog, and Reanalysis, Monthly Weather Review, 134, 657–663, https://doi.org/10.1175/MWR3088.1, 2006.

Massaoudi, M., Refaat, S. S., Chihi, I., Trabelsi, M., Oueslati, F. S., and Abu-Rub, H.: A novel stacked generalization ensemble-based hybrid LGBM-XGB-MLP model for Short-Term Load Forecasting, Energy, 214, 118874, https://doi.org/10.1016/j.energy.2020.118874, 2021.

Masson-Delmotte, V., Zhai, P., Pirani, A., Connors, S. L., Péan, C., Berger, S., Caud, N., Chen, Y., Goldfarb, L., and Gomis, M. I.: Climate change 2021: the physical science basis, Contribution of working group I to the sixth assessment report of the intergovernmental panel on climate change, 2, 2021.

Mearns, L. O., Rosenzweig, C., and Goldberg, R.: The effect of changes in daily and interannual climatic variability on CERES-Wheat: A sensitivity study, Climatic Change, 32, 257–292, https://doi.org/10.1007/BF00142465, 1996.

Meinshausen, M., Smith, S. J., Calvin, K., Daniel, J. S., Kainuma, M. L. T., Lamarque, J.-F., Matsumoto, K., Montzka, S. A., Raper, S. C. B., Riahi, K., Thomson, A., Velders, G. J. M., and van Vuuren, D. P. P.: The RCP greenhouse gas concentrations and their extensions from 1765 to 2300, Climatic Change, 109, 213, https://doi.org/10.1007/s10584-011-0156-z, 2011.

Moss, R. H., Edmonds, J. A., Hibbard, K. A., Manning, M. R., Rose, S. K., van Vuuren, D. P., Carter, T. R., Emori, S., Kainuma, M., Kram, T., Meehl, G. A., Mitchell, J. F. B., Nakicenovic, N., Riahi, K., Smith, S. J., Stouffer, R. J., Thomson, A. M., Weyant, J. P., and Wilbanks, T. J.: The next generation of scenarios for climate change research and assessment, Nature, 463, 747–756, https://doi.org/10.1038/nature08823, 2010.

Murphy, J.: Predictions of climate change over Europe using statistical and dynamical downscaling techniques, Int. J. Climatol., 20, 489–501, https://doi.org/10.1002/(SICI)1097-0088(200004)20:5<489::AID-JOC484>3.0.CO;2-6, 2000.

Mutz, S., Paeth, H., and Winkler, S.: Modelling of future mass balance changes of Norwegian glaciers by application of a dynamical–statistical model, Clim Dyn, 46, 1581–1597, https://doi.org/10.1007/s00382-015-2663-5, 2016.

Mutz, S. G. and Aschauer, J.: Empirical glacier mass-balance models for South America, J. Glaciol., 1–15, https://doi.org/10.1017/jog.2022.6, 2022.

Mutz, S. G., Scherrer, S., Muceniece, I., and Ehlers, T. A.: Twenty-first century regional temperature response in Chile based on empirical-statistical downscaling, Clim Dyn, 56, 2881–2894, https://doi.org/10.1007/s00382-020-05620-9, 2021.

Neal, R. M.: Bayesian learning for neural networks, Springer Science & Business Media, 2012.

Nourani, V., Razzaghzadeh, Z., Baghanam, A. H., and Molajou, A.: ANN-based statistical downscaling of climatic parameters using decision tree predictor screening method, Theor Appl Climatol, 137, 1729–1746, https://doi.org/10.1007/s00704-018-2686-z, 2019.

Opitz-Stapleton, S. and Gangopadhyay, S.: A non-parametric, statistical downscaling algorithm applied to the Rohini River Basin, Nepal, Theor Appl Climatol, 103, 375–386, https://doi.org/10.1007/s00704-010-0301-z, 2011.

Pachauri, R. K., Allen, M. R., Barros, V. R., Broome, J., Cramer, W., Christ, R., Church, J. A., Clarke, L., Dahe, Q., Dasgupta, P., Dubash, N. K., Edenhofer, O., Elgizouli, I., Field, C. B., Forster, P., Friedlingstein, P., Fuglestvedt, J., Gomez-Echeverri, L., Hallegatte, S., Hegerl, G., Howden, M., Jiang, K., Jimenez Cisneroz, B., Kattsov, V., Lee, H., Mach, K. J., Marotzke, J., Mastrandrea, M. D., Meyer, L., Minx, J., Mulugetta, Y., O'Brien, K., Oppenheimer, M., Pereira, J. J., Pichs-Madruga, R., Plattner, G.-K., Pörtner, H.-O., Power, S. B., Preston, B., Ravindranath, N. H., Reisinger, A., Riahi, K., Rusticucci, M.,

Scholes, R., Seyboth, K., Sokona, Y., Stavins, R., Stocker, T. F., Tschakert, P., van Vuuren, D., and van Ypserle, J.-P.: Climate Change 2014: Synthesis Report. Contribution of Working Groups I, II and III to the Fifth Assessment Report of the Intergovernmental Panel on Climate Change, edited by: Pachauri, R. K. and Meyer, L., IPCC, Geneva, Switzerland, 151 pp., 2014.

Padulano, R., Rianna, G., Costabile, P., Costanzo, C., Del Giudice, G., and Mercogliano, P.: Propagation of variability in climate projections within urban flood modelling: A multi-purpose impact analysis, Journal of Hydrology, 602, 126756, https://doi.org/10.1016/j.jhydrol.2021.126756, 2021.

Pal, S. K. and Mitra, S.: Multilayer perceptron, fuzzy sets, classifiaction, 1992.

Pang, B., Yue, J., Zhao, G., and Xu, Z.: Statistical Downscaling of Temperature with the Random Forest Model, Advances in Meteorology, 2017, e7265178, https://doi.org/10.1155/2017/7265178, 2017.

Paparrizos, S., Schindler, D., Potouridis, S., and Matzarakis, A.: Spatio-temporal analysis of present and future precipitation responses over South Germany, Journal of Water and Climate Change, 9, 490–499, https://doi.org/10.2166/wcc.2017.009, 2017.

Pedregosa, F., Varoquaux, G., Gramfort, A., Michel, V., Thirion, B., Grisel, O., Blondel, M., Prettenhofer, P., Weiss, R., Dubourg, V., Vanderplas, J., Passos, A., Cournapeau, D., Brucher, M., Perrot, M., and Duchesnay, É.: Scikit-learn: Machine Learning in Python, J. Mach. Learn. Res., 12, 2825–2830, 2011.

Picard, R. R. and Cook, R. D.: Cross-Validation of Regression Models, Journal of the American Statistical Association, 79, 575–583, https://doi.org/10.1080/01621459.1984.10478083, 1984.

Pontes, F. J., Amorim, G. F., Balestrassi, P. P., Paiva, A. P., and Ferreira, J. R.: Design of experiments and focused grid search for neural network parameter optimization, Neurocomputing, 186, 22–34, https://doi.org/10.1016/j.neucom.2015.12.061, 2016.

Quesada-Chacón, D., Barfus, K., and Bernhofer, C.: Repeatable high-resolution statistical downscaling through deep learning, Geoscientific Model Development, 15, 7353–7370, https://doi.org/10.5194/gmd-15-7353-2022, 2022.

Quinlan, J. R.: Bagging, boosting, and C4.S, in: Proceedings of the thirteenth national conference on Artificial intelligence - Volume 1, Portland, Oregon, 725–730, 1996.

Raissi, M. and Karniadakis, G. E.: Hidden physics models: Machine learning of nonlinear partial differential equations, Journal of Computational Physics, 357, 125–141, https://doi.org/10.1016/j.jcp.2017.11.039, 2018.

Ramon, J., Lledó, L., Bretonnière, P.-A., Samsó, M., and Doblas-Reyes, F. J.: A perfect prognosis downscaling methodology for seasonal prediction of local-scale wind speeds, Environ. Res. Lett., 16, 054010, https://doi.org/10.1088/1748-9326/abe491, 2021.

Reichert, B. K., Bengtsson, L., and Åkesson, O.: A statistical modeling approach for the simulation of local paleoclimatic proxy records using general circulation model output, Journal of Geophysical Research: Atmospheres, 104, 19071–19083, https://doi.org/10.1029/1999JD900264, 1999.

1195 Reid, S. and Grudic, G.: Regularized Linear Models in Stacked Generalization, in: Multiple Classifier Systems, Berlin, Heidelberg, 112–121, https://doi.org/10.1007/978-3-642-02326-2_12, 2009.

Rumelhart, D. E., Hinton, G. E., and Williams, R. J.: Learning representations by back-propagating errors, nature, 323, 533–536, 1986.

Sachindra, D. A., Huang, F., Barton, A., and Perera, B. J. C.: Statistical downscaling of general circulation model outputs to

1200 precipitation—part 2: bias-correction and future projections, International Journal of Climatology, 34, 3282–3303, https://doi.org/10.1002/joc.3915, 2014.

Sachindra, D. A., Ahmed, K., Rashid, Md. M., Shahid, S., and Perera, B. J. C.: Statistical downscaling of precipitation using machine learning techniques, Atmospheric Research, 212, 240–258, https://doi.org/10.1016/j.atmosres.2018.05.022, 2018.

San-Martín, D., Cofiño, A. S., Herrera, S., and Gutiérrez, J. M.: The ENSEMBLES statistical downscaling portal. An end-to-

1205 end tool for regional impact studies, 2014.

Schapire, R. E.: A brief introduction to boosting, in: Ijcai, 1401–1406, 1999.

Schapire, R. E.: The boosting approach to machine learning: An overview, Nonlinear estimation and classification, 149–171, 2003.

Schapire, R. E. and Freund, Y.: Boosting: Foundations and algorithms, Kybernetes, 2013.

1210 Schmidli, J., Goodess, C. M., Frei, C., Haylock, M. R., Hundecha, Y., Ribalaygua, J., and Schmith, T.: Statistical and dynamical downscaling of precipitation: An evaluation and comparison of scenarios for the European Alps, J. Geophys. Res., 112, D04105, https://doi.org/10.1029/2005JD007026, 2007.

Selle, B., Rink, K., and Kolditz, O.: Recharge and discharge controls on groundwater travel times and flow paths to production wells for the Ammer catchment in southwestern Germany, Environ Earth Sci, 69, 443–452, https://doi.org/10.1007/s12665-

1215 013-2333-z, 2013.

Shahhosseini, M., Hu, G., and Archontoulis, S. V.: Forecasting Corn Yield With Machine Learning Ensembles, Front. Plant Sci., 11, 1120, https://doi.org/10.3389/fpls.2020.01120, 2020.

Shepherd, T. G.: Atmospheric circulation as a source of uncertainty in climate change projections, Nature Geosci, 7, 703–708, https://doi.org/10.1038/ngeo2253, 2014.

1220 Snoek, J., Larochelle, H., and Adams, R. P.: Practical bayesian optimization of machine learning algorithms, Advances in neural information processing systems, 25, 2012.

Steppeler, J., Doms, G., Schättler, U., Bitzer, H. W., Gassmann, A., Damrath, U., and Gregoric, G.: Meso-gamma scale forecasts using the nonhydrostatic model LM, Meteorol Atmos Phys, 82, 75–96, https://doi.org/10.1007/s00703-001-0592-9, 2003.

1225 Sterl, A.: On the (In)Homogeneity of Reanalysis Products, Journal of Climate, 17, 3866–3873, https://doi.org/10.1175/1520-0442(2004)017<3866:OTIORP>2.0.CO;2, 2004.

Stone, M.: Cross-Validatory Choice and Assessment of Statistical Predictions (With Discussion), Journal of the Royal Statistical Society: Series B (Methodological), 38, 102–102, https://doi.org/10.1111/j.2517-6161.1976.tb01573.x, 1976.

Storch, H. von and Zwiers, F. W.: Statistical Analysis in Climate Research, Cambridge University Press, 995 pp., 2002.

1230 Sunyer, M. A., Gregersen, I. B., Rosbjerg, D., Madsen, H., Luchner, J., and Arnbjerg-Nielsen, K.: Comparison of different statistical downscaling methods to estimate changes in hourly extreme precipitation using RCM projections from ENSEMBLES, International Journal of Climatology, 35, 2528–2539, https://doi.org/10.1002/joc.4138, 2015.

Tatli, H., Nüzhet Dalfes, H., and Sibel Menteş, Ş.: A statistical downscaling method for monthly total precipitation over Turkey, International Journal of Climatology, 24, 161–180, https://doi.org/10.1002/joc.997, 2004.

1235 Taylor, K. E., Stouffer, R. J., and Meehl, G. A.: An Overview of CMIP5 and the Experiment Design, Bulletin of the American Meteorological Society, 93, 485–498, https://doi.org/10.1175/BAMS-D-11-00094.1, 2012.

Thompson, A. J., Tabor, C. R., Poulsen, C. J., and Skinner, C. B.: Water isotopic constraints on the enhancement of the mid-Holocene West African monsoon, Earth and Planetary Science Letters, 554, 116677, https://doi.org/10.1016/j.epsl.2020.116677, 2021.

1240 Tibshirani, R.: Regression Shrinkage and Selection Via the Lasso, Journal of the Royal Statistical Society: Series B (Methodological), 58, 267–288, https://doi.org/10.1111/j.2517-6161.1996.tb02080.x, 1996.

Ting, K. M. and Witten, I. H.: Issues in Stacked Generalization, Journal of Artificial Intelligence Research, 10, 271–289, https://doi.org/10.1613/jair.594, 1999.

Tipping, M. E.: Sparse Bayesian learning and the relevance vector machine, Journal of machine learning research, 1, 211–244, 1245 2001.

Tripathi, S., Srinivas, V. V., and Nanjundiah, R. S.: Downscaling of precipitation for climate change scenarios: A support vector machine approach, Journal of Hydrology, 330, 621–640, https://doi.org/10.1016/j.jhydrol.2006.04.030, 2006.

Vapnik, V.: The nature of statistical learning theory, Springer science & business media, 1999.

Vrac, M., Marbaix, P., Paillard, D., and Naveau, P.: Non-linear statistical downscaling of present and LGM precipitation and 1250 temperatures over Europe, Climate of the Past, 3, 669–682, https://doi.org/10.5194/cp-3-669-2007, 2007.

Vu, M. T., Aribarg, T., Supratid, S., Raghavan, S. V., and Liong, S.-Y.: Statistical downscaling rainfall using artificial neural network: significantly wetter Bangkok?, Theor Appl Climatol, 126, 453–467, https://doi.org/10.1007/s00704-015-1580-1, 2016.

Weaver, C. P., Lempert, R. J., Brown, C., Hall, J. A., Revell, D., and Sarewitz, D.: Improving the contribution of climate 1255 model information to decision making: the value and demands of robust decision frameworks, WIREs Climate Change, 4, 39–60, https://doi.org/10.1002/wcc.202, 2013.

Wilby, R. L. and Dawson, C. W.: The Statistical DownScaling Model: insights from one decade of application, International Journal of Climatology, 33, 1707–1719, https://doi.org/10.1002/joc.3544, 2013.

Wilby, R. L. and Wigley, T. M. L.: Future changes in the distribution of daily precipitation totals across North America, 1260 Geophysical Research Letters, 29, 39-1-39–4, https://doi.org/10.1029/2001GL013048, 2002.

Wilby, R. L., Wigley, T. M. L., Conway, D., Jones, P. D., Hewitson, B. C., Main, J., and Wilks, D. S.: Statistical downscaling of general circulation model output: A comparison of methods, Water Resources Research, 34, 2995–3008, https://doi.org/10.1029/98WR02577, 1998.

Wilby, R. L., Dawson, C. W., and Barrow, E. M.: sdsm — a decision support tool for the assessment of regional climate change impacts, Environmental Modelling & Software, 17, 145–157, https://doi.org/10.1016/S1364-8152(01)00060-3, 2002.

Wilby, R. L., Charles, S. P., Zorita, E., Timbal, B., Whetton, P., and Mearns, L. O.: Guidelines for use of climate scenarios developed from statistical downscaling methods, Supporting material of the Intergovernmental Panel on Climate Change, available from the DDC of IPCC TGCIA, 27, 2004.

Wilks, D. S.: Statistical methods in the atmospheric sciences, Academic press, 2011.

Wipf, D. and Nagarajan, S.: A new view of automatic relevance determination, Advances in neural information processing systems, 20, 2007.

Wolpert, D. H.: Stacked generalization, Neural Networks, 5, 241–259, https://doi.org/10.1016/S0893-6080(05)80023-1, 1992.

Wu, T. T. and Lange, K.: Coordinate descent algorithms for lasso penalized regression, The Annals of Applied Statistics, 2, 224–244, https://doi.org/10.1214/07-AOAS147, 2008.

Xu, R., Chen, N., Chen, Y., and Chen, Z.: Downscaling and Projection of Multi-CMIP5 Precipitation Using Machine Learning Methods in the Upper Han River Basin, Advances in Meteorology, 2020, e8680436, https://doi.org/10.1155/2020/8680436, 2020.

Xu, Z., Han, Y., and Yang, Z.: Dynamical downscaling of regional climate: A review of methods and limitations, Sci. China Earth Sci., 62, 365–375, https://doi.org/10.1007/s11430-018-9261-5, 2019.

Zhang, C. and Ma, Y.: Ensemble machine learning: methods and applications, Springer, 2012.

Zhang, J., Liu, K., and Wang, M.: Downscaling Groundwater Storage Data in China to a 1-km Resolution Using Machine Learning Methods, Remote Sensing, 13, 523, https://doi.org/10.3390/rs13030523, 2021.

Zhang, X. and Yan, X.: A new statistical precipitation downscaling method with Bayesian model averaging: a case study in China, Clim Dyn, 45, 2541–2555, https://doi.org/10.1007/s00382-015-2491-7, 2015.

Zhou, H., Zhang, J., Zhou, Y., Guo, X., and Ma, Y.: A feature selection algorithm of decision tree based on feature weight, Expert Systems with Applications, 164, 113842, https://doi.org/10.1016/j.eswa.2020.113842, 2021.

Zorita, E. and Storch, H. von: The Analog Method as a Simple Statistical Downscaling Technique: Comparison with More Complicated Methods, Journal of Climate, 12, 2474–2489, https://doi.org/10.1175/1520-0442(1999)012<2474:TAMAAS>2.0.CO;2, 1999.